The following publication Mansour, Ahmed; Ye, Junhua; Li, Yaxin; Luo, Huan; Wang, Jingxian; Weng, Duojie; Chen, Wu(2023). Everywhere: A Framework for Ubiquitous Indoor Localization. IEEE Internet of Things Journal, 10(6), 5095-5113 is available at https://doi.org/10.1109/JIOT.2022.3222003.

Everywhere: A Framework for Ubiquitous Indoor Localization

Ahmed Mansour, Junhua Ye, Yaxin Li, Huan Luo, Jingxian Wang, Duojie Weng, and Wu Chen

***Abstract*— Smartphones have become an integral part of daily human life and enable almost unlimited coverage of human mobility. Thus, collecting pervasive crowdsourced signatures is feasible. Autonomous localization of such signatures promotes the development of a self-deployable and ubiquitous Indoor Positioning System (IPS). However, previous IPSs-based crowdsourcing have not considered leveraging such data for developing ubiquitous IPSs. They have relied on methods for data selection and sources for localization adjustment that could work against realizing a ubiquitous system. In contrast, this study introduces a framework "*Everywhere*" that leverages crowdsourced data to develop a ubiquitous IPS and addresses existing challenges while developing such systems. Particularly, inertial data selection criteria are proposed to autonomously generate traces with better localization. Moreover, pervasive GNSS data are leveraged to adjust trace localization, while simultaneously introducing a deploying location (inside elevators) of one anchor node. The node surveys all the floors while reducing the localization error, especially for the buildings surrounded by GNSS-denied areas. Additionally, cumulative data densification is leveraged to realize pervasive resources within the building, thereby boosting trace adjustment and extending database spatial coverage. Furthermore, a better selection of neighboring fingerprints is proposed to enhance online fingerprinting. Such a framework can promote a ubiquitous IPS development for buildings regardless of whether they are surrounded by open sky or GNSS-denied areas.**

***Index Terms*—Crowdsourcing, fingerprinting, indoor localization, Internet of Things (IoT), Location-Based Service (LBS), and ubiquitous localization.**

I. INTRODUCTION

The rapid development of smart life and embedded sensors in Internet of Things (IoT) devices has led to a significant demand for location-based services (LBSs). Consequently, ubiquitous localization has become the primary objective of localization technologies [1] to meet the future needs of LBS in next-generation smart cities [2]. Moreover, with the advancement of IoT, ubiquitous localization becomes crucial for both consumers and service providers to obtain reliable localization information anytime and everywhere [3]. Global navigation satellite systems (GNSS) can provide accurate LBS in open-sky areas [1]. However, the performance of GNSS deteriorates indoors because of signal blockage and attenuation. In contrast to outdoor localization, relying on one technology to provide a reliable solution for different indoor LBS remains unfeasible [3].

Over the past two decades, several technologies were proposed to realize efficient indoor positioning systems (IPSs) [4]. These technologies can be broadly divided into two main categories: infrastructure-free and infrastructure-based technologies. In the former category, the system localizes a user without using building resources [3], such as inertial sensors and GNSS. In contrast, the latter category of systems exploits building resources, such as floor plans and wireless signals. Wireless-based technologies can be further divided into two subgroups:1) pervasive signals, such as WiFi-based received signal strength (RSS) and magnetic field (MF), and 2) signals-based auxiliary resources, such as Bluetooth low energy (BLE), ultra-wide band, and infrared signals. Generally, system-based auxiliary technologies can achieve more accurate performance; however, the low cost and high scalability of infrastructure-free and opportunistic signals are considerably beneficial in the development of ubiquitous systems [4].

Based on off-the-shelf inertial sensors, pedestrian dead reckoning (PDR) can provide reliable short-term localization and support the development of self-deployable IPS by bridging the wireless localization outages [5]. Smartphone richness with multiple sensors enables the measurement of pervasive signals (*e.g.*, WiFi-based RSS and MF) and their utilization to update the PDR solution [6]. Leveraging these measurements using fingerprinting-based positioning methods provides an accurate solution compared to multitrilateration methods because the former mitigates multipath effects [6]. However, manual training and updating of offline fingerprinting databases are time-consuming and labor-intensive, and limit the scalability of such ubiquitous technologies [7]. Thus, the autonomous generation of these databases can help to leverage pervasive technologies in developing self-deployable systems.

This research was funded by Shenzhen Science and Technology Innovation Commission (grant number: JCYJ20170818104822282) and Hong Kong Research Grants Council (RGC) Competitive Earmarked Research Grants (Project No: PolyU 152151/17E). It is also supported by the Smart City Research Institute of Hong Kong Polytechnic University. (*Corresponding author: Wu Chen*)

A. Mansour is with Department of Land Surveying and Geo-Informatics, The Hong Kong Polytechnic University, Hong Kong (email: ahmed.m.mostafa@connect.polyu.hk)

H. Luo, J. Wang and D. Weng are with Department of Land Surveying and Geo-Informatics, The Hong Kong Polytechnic University, Hong Kong.

W. Chen and Y. Li are with Shenzhen Research Institute, The Hong Kong Polytechnic University, Shenzhen 518057, China and Department of Land Surveying and Geo-Informatics, The Hong Kong Polytechnic University, Hong Kong.

J. Ye is with College of Environment and Resources, Zhejiang A&F University, Hangzhou 311300, China.

Crowdsourcing, which is the process of harnessing the power of thousands of users to perform a specific task, has been studied to eliminate human-supervised approaches. Human supervision for databases can be eliminated by leveraging *regular users*, instead of *experts*, to produce offline databases [4]. In an ideal situation, the absolute locations of the indoor signatures can be estimated consecutively using PDR and the accurate outdoors GNSS locations (*i.e.*, which can act as anchor nodes (AN)) when a user moves from outdoors to indoors or vice versa. However, in scenarios where GNSS-denied areas surround a building (*e.g.*, in deep urban canyons), obtaining accurate outdoor GNSS data to act as outer (*i.e.*, outside the building) ANs is unfeasible [8]. Moreover, collecting data using freely moving users can result in unqualified inertial data, which hinders the creation of traces with better localization [9]. However, despite using qualified inertial data, PDR problems such as accumulated heading drift and sensor bias reduce its reliability. In particular, PDR cannot be expected to reliably estimate the positions of the extracted fingerprints on its own without calibration sources [10].

Autonomous localization of pervasive signatures promotes the development of self-deployable and ubiquitous IPS. However, previous crowdsourcing studies have not paid attention to the overarching aim of leveraging this data. Their methods potentially hinder the ubiquity of their systems owing to several limitations. Firstly, the data selection criteria used to autonomously generate traces with improved localization were insufficient. Although a few studies [10, 11] have introduced factors to assess the data quality depending on the availability of auxiliary resources, a majority of the studies considered that all collected data were qualified to contribute, which could deteriorate the quality of the generated databases. Secondly, the sources utilized for trace localization adjustment could potentially hinder the realization of a ubiquitous system. To be precise, certain studies [12-14] considered imperative participation from active and experienced users. Several systems [7, 14, 15] assumed that floor plans are always available to correct collected traces. Other systems [10, 11, 16] densely equipped each floor with auxiliary internal (*i.e.*, within the floor area) ANs, instead of leveraging pervasive resources. A few systems [17] relied only on accurate GNSS data; however, such systems could be exposed to a high margin of localization error, especially for buildings surrounded by GNSS-denied areas [8]. Thirdly, to estimate online positioning-based fingerprinting, most existing matching methods utilize the similarities between offline and online signatures to the best neighboring reference points (RPs) [6]. However, these signatures are highly susceptible to mismatches owing to the characteristics of the signals and indoor environments, even when the offline signatures are statically trained by experts [4]. Such mismatches can be aggravated when utilizing crowdsourced signatures collected by different smartphones from freely moving users.

Our proposed framework is aimed at developing a low-cost, self-deployable, and ubiquitous IPS that can be used for buildings surrounded by either GNSS-denied or open-sky areas. The proposed framework relies on multisensory integration and comprises both online and offline engines (Fig. 1). The online engine comprises an integrated solution-based extended Kalman filter (EKF) to fuse fingerprinting and PDR solutions. The offline engine comprises a scheme for autonomous generation of the requirements of the fingerprinting solution (i.e., radio and magnetic maps). The proposed offline engine easily converts regular users into efficient producers of these requirements. Furthermore, the engine operates without dependency on resources that could limit the system's ubiquity, such as floor plans, waiting for the participation of active and experienced users, or the cumbersome deployment of BLE ANs at each floor in the building.

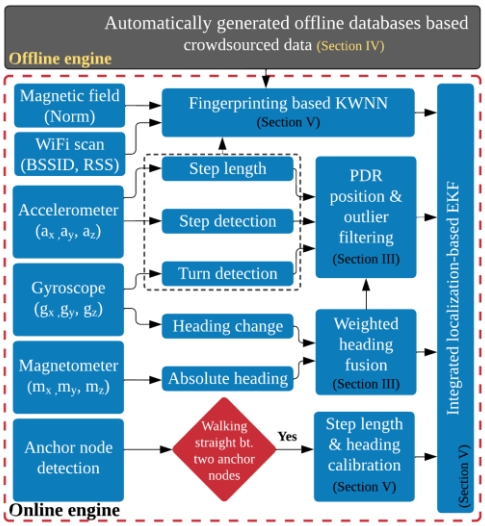

Fig. 1. *Everywhere* architecture.

As aforementioned, IPSs are largely ubiquity-limited by offline fingerprinting requirements, thereby the majority of our study *contributions* serve the offline engine. Compared to the existing crowdsourced-IPSs, our study makes the following contributions: we introduced selection criteria to qualify inertial data. These criteria depend mainly on the characteristics of the collected data and do not rely on factors that require the deployment of internal auxiliary ANs or floor plans (i.e., as suggested in previous studies), thereby maintaining the system's ubiquity. In addition, the large errors expected while depending on GNSS ANs to localize crowdsourced signatures in buildings surrounded by GNSS-denied areas or multistory buildings are mitigated by proposing leveraging the elevators as a source of detecting or deploying AN. The proposed location provides a trade-off solution that maintains a high localization accuracy at all floors with low deployment cost and effort. Precisely, AN can be detected at all floors with cost minimized by a factor of N:1, where N is the number of floors. ANs such as BLE beacons can be effortlessly deployed in existing building elevators or incorporated into elevators as a pre-installed component, similar to security cameras. Furthermore, we proposed leveraging the data accumulation over time to autonomously derive the identifiers, locations, and propagation information of fixed WiFi APs to act as internal ANs and eliminate the need to deploy auxiliary ANs at each

floor. Inferences from these pervasive ANs help align the traces collected entirely within the floor area, thereby improving trace localization, and extending the spatial coverage of the generated databases. In the online phase, the generated radio and magnetic maps were utilized to estimate fingerprinting solution. Before fusing fingerprinting and PDR solutions, we proposed leveraging the reliable relative PDR displacement and gyro heading change to boost the selection of the best nearest neighboring RPs while walking in straight portions. Detecting these portions between successive ANs was also leveraged to calibrate step length, control gyro heading drift, and filter PDR outliers.

The remainder of this paper is organized as follows. Section II reviews related works. Sections III, IV, and V discuss the proposed methods for track generation, autonomous offline database establishment, and online positioning. The experiments, results, and evaluations are presented in Section VI, followed by the conclusion and future scope in Section VII.

II. Related Work

A. Offline Databases Based on Crowdsourced Data

The reliance on pervasive resources to achieve a ubiquitous IPSs makes addressing the challenges of crowdsourcing systems more difficult. This section sheds light on how related studies have addressed crowdsourcing challenges. TABLE **I** summarizes the differences among recent studies developed using infrastructure-free, opportunistic signals, floor plans, and BLE beacons, as well as the strengths and limitations of these studies regarding the development of a ubiquitous system.

1) Selecting Qualified Inertial Data

Massive errors are expected in databases generated from data collected by different smartphone models with different sensor capabilities from freely moving users with different walking behaviors, body profiles, and walking speeds [9]. Users may also use different poses when carrying their smartphones, such as horizontal holding, calling, or swinging; the devices could also be in pockets or bags during the daily activities of the users. The flexible portability of handheld devices is another source of error, especially when estimating attitude angles [18]. Accordingly, to develop a self-deployable system, qualified data must be autonomously selected to generate traces with better localization. From the perspective of big data, even a modest quantity of qualified data is sufficient to create qualified databases [9]. Therefore, only trustworthy data must be used to maintain database quality.

Importantly, the quality of inertial data can be ensured only by generating traces with geometric shapes similar to the ones that are actually occurred by users. The combination of all such traces guarantees improved localization performance and consistent signatures. Several crowdsourced studies [9, 12, 15, 17, 19] considered all collected data in database generation and directly adjusted the collected traces depending on the auxiliary sources; however, these auxiliary sources may not be available while developing a ubiquitous system. However, from the perspective of big data [10], considering traces with unqualified data can degrade the quality of the generated databases regardless of the adjustment source used.

Zhang, et al. [10] proposed an early quantitative framework to evaluate the quality of crowdsourced inertial data without user intervention. They introduced factors such as the collection time, gyro errors, and smartphone motion mode, and weighted the contribution of each factor to estimate a quality score for each collected trace. They assigned the highest weight to the collection duration factor to avoid the accumulated heading drift of long tracks and the errors arising from more collection. Yu, et al. [11] proposed a similar approach with factors such as the trace lengths and the similarity between the generated and adjusted traces. However, their similarity factor assessed the adjustment method instead of the inertial data quality; thus, unqualified traces could contribute to the generation and affect the overall database quality.

Notably, in [10, 11], dense auxiliary internal ANs were deployed to augment the chances of finding short tracks between ANs. Although tracks with short lengths/durations were found to be trustworthy, their inertial data quality may be insufficient for accurate localization performance. Additionally, in the absence of dense auxiliary internal ANs (*i.e.*, ubiquitous systems), long traces are expected between outer ANs, especially for large-scale buildings. Thus, reliance on short traces that depend on auxiliary internal ANs could hinder the development of a ubiquitous system. In the initial stages of databases generation, checking the quality of the traces collected between outer ANs and considering those entirely collected with qualified data regardless of their lengths, could eliminate the need for deploying auxiliary internal ANs. Moreover, the densification of such traces over time could help infer pervasive adjustment resources (*e.g.*, fixed WiFi ANs). Such internal resources could contribute to adjusting the traces collected entirely within the floor in the following database generation stages, extending the spatial coverage, and enhancing the quality of the initially generated databases.

2) Adjusting the Traces Localization

In related literature, three sources are commonly used to adjust the localization of the collected traces. The data collectors are the first source. In several studies, researchers provided data collectors with specific instructions, turning autonomous generation into a semi-supervised creation. Lohan, et al. [13] asked data collectors to provide feedback regarding their estimated positions. Databases created by Lohan, et al. [13] were also utilized in [12]. Santos, et al. [14] instructed users to walk along specific paths. However, such methods require the participation of active and experienced users, which cannot be guaranteed in real-world scenarios, thereby limiting the ubiquity of such systems. The floor plans of buildings are the second source. Several studies have assumed that floor plans are always available and can be used to correct the collected traces. For example, Rai, et al. [7] developed a Zee system that utilized floor plans to resolve RP position ambiguity. Gu, et al. [15] leveraged floor plans to create a landmark graph. Santos, et al. [14] estimated the locations of RPs using floor plans and geomagnetic similarities between

TABLE I
COMPARISON AMONG RECENT INDOOR LOCALIZATION SYSTEMS BASED ON CROWDSOURCING

Study	Infrastructure-Free		Infrastructure-Based			Fingerprinting		Remarks regarding developing a self-deployable system
						Offline	Online	
	GNSS	Inertial sensors	Pervasive Signals	BLE ANs Density and distribution	Floor plans	Autonomous	Matching method	
[14]	✗	✓	WiFi✓ MF✓	**No need**	**Need**	**Semi-supervised**	Particle Filter	**Strengths**: the use of pervasive signals and trace adjusting-based geomagnetic similarities. **Limitations**: depended on floor maps and instructing users.
LG-Loc [15]	✓	✓	WiFi✓ Light✓	**No need**	**Need**	✓	Graph matching	**Strengths**: exploiting natural landmarks and GNSS data. **Limitations**: the dependency on floor plans.
[12]	✓	✓	WiFi✓	**No need**	**No need**	**Semi-supervised**	Clustering	**Strengths**: using pervasive signals. **Limitations**: the dependency on the users' feedback to correct the traces ad considering the entire collected data can contribute (no criteria for qualified data selection).
[19]	✓	✓	WiFi✓	**No need**	**No need**	**Semi-supervised**	Probabilistic (Gaussian distribution)	**Strengths**: the use of accurate GNSS data as ANs. **Limitations**: Manual distinguishing the gates and significant localization errors for the buildings surrounded by GNSS-denied areas.
SoiCP [17]	✓	✓	WiFi✓	**No need**	**No need**	✓	Deterministic-based KWNN	**Strengths**: using accurate GNSS data as ANs and proposing three layers of trace matching. **Limitations**: buildings surrounded by GNSS-denied areas are prone to significant localization errors.
3D-CSWS [11]	✗	✓	WiFi✓	**High** 6 units per 2 floors	**No need**	✓	Deterministic-based KWNN	**Strengths**: introducing factors for selecting the qualified data. **Limitations**: use BLE ANs inside each floor, which is costly and labor-intensive, especially for multi-story buildings.
[9]	✓	✓	WiFi✓ MF✓	**Stated but not clarified**	**No need**	✓	Probabilistic (Gaussian distribution)	**Strengths**: Introducing fingerprinting accuracy indicators. **Limitations**: considering the entire collected data (no criteria for qualified data selection).
[10]	✓	✓	WiFi✓	**High** 10 units per floor	**No need**	✓	Deterministic-based KNN	**Strengths**: establishing criteria for selecting inertial data. **Limitations**: the use of dense BLE ANs inside each floor is costly and labor-intensive.
Our proposed system	✓	✓	WiFi✓ MF✓	***Low & serve the whole floors***	**No need**	✓	KWNN based-***enhanced RPs selection criteria***	**Strengths:** exploiting GNSS data, using one AN location to survey the entire floors, reducing the localization error for the building surrounded by GNSS-denied areas, inferring fixed WiFi APs to act as internal ANs, selecting qualified inertial data autonomously, and enhancing online fingerprinting. **Limitations:** the proposed post-data processes are crucial to improving localization accuracy; however, the data collection process is also important to ensure the applicability and widespread of such crowdsourced methods. User-friendly data collection strategies and privacy guarantees are required to ensure widespread adoption.

straight traces. However, the unavailability of such plans due to several reasons (*e.g.*, privacy concerns and missing data) could limit the ubiquity of such systems. Finally, anchor nodes are the third source. Two sources of ANs are utilized to correct the PDR traces: accurate GNSS data and BLE beacons.

With respect to the first AN source, Yu, et al. [19] used the gate locations to initialize the PDR traces. They distinguished the gates by observing the significant change in the GNSS signals when moving indoors from outside and manually collected the WiFi access points (APs) data at each entrance. The SoiCP system developed by Li, et al. [17] leveraged building gates and their WiFi signatures as features to adjust noisy crowdsourcing traces. Using only GNSS as ANs may be reasonable for buildings surrounded by open-sky areas; however, in urban canyons, the building entrances in GNSS-denied areas are susceptible to a large error margin [20]. Additionally, in complex buildings (*i.e.*, with large-scale areas and multiple levels), the heading drift of long paths can be aggravated until users reach the gates, thereby affecting localization accuracy of the extracted signatures. Consequently, recent crowdsourced-IPSs have installed auxiliary ANs at known locations within building floors to overcome the aforementioned limitations. In contrast, BLE beacons possess several advantages, such as compatibility with different IoT devices, low cost, and low coverage range (*i.e.*, precise localization). Therefore, most crowdsourced IPSs select them to deploy internal ANs. Zhang, et al. [10] distributed ten BLE internal ANs inside a shopping mall floor. Similarly, Yu, et al. [11] distributed six beacons on two floors to correct PDR traces and achieve 3D positioning. Kotrotsios and Orphanoudakis [21] deployed an AN every 6 m^2 to achieve meter-level accuracy. Yu, et al. [16] deployed BLE beacons at intervals of 7.0 m to replace pervasive WiFi signatures using BLE RSS signatures. However, a close analysis of these studies reveals that the beacons were densely deployed at each building level without considering the overall cost and deployment efforts, thereby limiting the ubiquity of the systems.

B. Online Position Estimation Based on Fingerprinting

Numerous matching algorithms have been proposed for online localization based on fingerprinting. Bahl and Padmanabhan [22] developed the first RSS-based system (RADAR) using a deterministic method. Youssef and Agrawala [23] proposed a Horus system using a K-nearest neighbors-based probabilistic method. Machine learning methods such as random forest [24] and neural networks [25] have also been proposed to improve fingerprinting performance. Compared with previous point-to-point matching approaches, Li, et al. [26] introduced profile matching-based dynamic time warping to extend the observation dimensionality. Such studies have utilized the similarity between online and offline signatures to select the best K-neighboring RPs. However, even with manual training approaches, these signatures are highly susceptible to variations and mismatches, owing to the characteristics of the signals and indoor environments. Such discrepancies could worsen when crowdsourced databases created by different smartphones and freely moving users are used. Consequently, augmented selection criteria for the best K-neighboring RPs should be considered to reduce mismatches and improve online fingerprinting, particularly for crowdsource-based databases.

III. Walking Track Generation Based on PDR

This section briefly illustrates the PDR components employed to generate walking tracks from the crowdsourced data, establish the fusion model in EKF, and participate in selecting the best neighboring RPs in the online fingerprinting stage. Four components were considered in the PDR mechanism including step detection, step length estimation, heading determination, and outlier filtering after detecting straight portions and turns.

Regarding step detection, the triggered steps were detected by capturing the peak and valley of the vertical acceleration relative to the surface of the Earth. Notably, these extremes can be formed during pedestrian walk regardless of the device pose [27]. The gravity effect was first subtracted to determine the linear acceleration. A low-pass filter was then applied to reduce the noise effect. The procedures of the proposed detection method comprised three conditions to robustly determine the peak and valley points of each step including:1) the extreme of each part should exceed a certain threshold (e.g., 0.65 m/s^2). This threshold enables excluding simple hand trembling from counting as a step; 2) since the gait cycle typically lasts between 0.2-1.6 s depending on the walking speed, the step duration should last a certain interval (e.g., 100 ms); and 3) a valley and vice versa preceded each peak. Moreover, owing to acceleration jitter, false peaks/valleys could occur in a short time interval with acceleration above the predefined threshold. A short time window was applied to filter out these false extremes. The length of each triggered step was then estimated using the a non-linear empirical approach proposed in [28]. This approach assumes that the step length is correlated with the total vertical acceleration change of the step. The length sl_k of the k^{th} step was estimated based on the following expression:

$$sl_k = m \sqrt[4]{a_{peak,k}^{ncs} - a_{valley,k}^{ncs}}, \quad 0.6 \le sl_k \le 0.9 \quad (1)$$

where $a_{peak,k}^{ncs}$ and $a_{valley,k}^{ncs}$ are the filtered acceleration of the step peak and valley, respectively. m is a parameter related to the profile of the pedestrian. Herein, m is initialized equal to 0.55. Then a calibrated step length was obtained when a user walked in a straight line between two ANs. The calibrated step length updated the EKF model (refer to Section V.B).

A weighted fusion algorithm [29] was used to leverage the high reliability of short-term gyro relative heading and the trustworthy absolute compass heading at the quasi-static magnetic field (QSMF) periods. The contribution of each source was controlled based on two factors: 1) the correlation between the two sources, and 2) the availability of QSMF periods. Among the magnetic, gyro integral, and previous step headings, the best candidates were selected to contribute part of their weights. Furthermore, a heading calibration based on detecting two successive ANs while walking in a straight line was used to calibrate the estimated heading and update the EKF (refer to Section V.B).

Once a step is triggered, a PDR mechanism can estimate its length and heading, then the coordinates of the current step can be computed based on the position of the previous step. When a pedestrian walks in a straight line, there should be no significant change in the heading of the adjacent steps unless an actual turn occurs. However, unexpected device shaking can cause substantial variation in the estimated position. To curb that, we incorporated a turn detection method and outlier filtering mechanism into the PDR approach. The following procedures were conducted to detect the turns and straight portions, and filter the outliers. The change in gyro heading was firstly smoothed. Subsequently, a sliding window was applied, and the maximum difference of the smoothed change within this window (Δh_{max}) was recursively monitored. Δh_{max} was used to detect the turn intervals and events, and decide whether a triggered step was a part of a turning or straight walking intervals. A real-time turn detection algorithm was developed using a decision tree based on lower and higher thresholds for Δh_{max}, (i.e., λ_l and λ_h, respectively). λ_l was employed as the allowable margin of heading change during walking in a straight line. A test was implemented by walking in a straight corridor several times to determine the range of λ_l. λ_h was employed as the minimum total heading change required to consider a rotation as a turn.

Intuitively, Δh_{max} should be almost zero during walking in a straight line; thus, while it did not exceed λ_l, we considered the user walked in a straight line (see Fig. 2) and attributed the variation of Δh_{max} to the device shaking. The PDR locations of the triggered steps during this period were supposed to lie on a straight line; thus, the RANSAC method [30] was used to estimate the linear model parameters (a, b, c). Subsequently, we calculated the perpendicular distance (n) (i.e., from the estimated PDR location (x_k, y_k) of step k to the RANSAC linear model) as follows:

$$n = \left| \frac{ax_k + by_k + c}{\sqrt{a^2 + b^2}} \right| \quad (2)$$

If n was lower than a predefined threshold (*e.g.*, 1.5 m), the estimated step position was added to the line points, and the RANSAC algorithm was iterated to re-estimate the line parameters. Otherwise, the estimated PDR position of this step was adjusted as follows:

$$\begin{bmatrix} \hat{x}_k \\ \hat{y}_k \end{bmatrix} = \begin{bmatrix} x_k - \frac{a}{a^2+b^2}(ax_k + by_k + c) \\ \frac{-a}{b}\hat{x}_k - \frac{c}{b} \end{bmatrix} \quad (3)$$

In contrast, when Δh_{max} exceeded λ_l, a sign of turning was triggered, yet the algorithm still did not consider it as a turn until observing the subsequent values of Δh_{max}. If it then declined, the algorithm did not trigger turn, but initialized a new linear model because a slight change in the walking heading occurred. But, if Δh_{max} continued raising and exceeded λ_h, a turn was triggered, and a new linear model was also initialized.

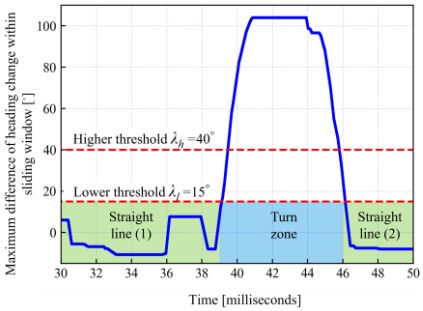

Fig. 2. Maximum difference of the gyroscope's heading change within a sliding window.

IV. Offline Fingerprinting Databases Generation

This section illustrates the proposed scheme for generating offline radio and magnetic maps without human supervision, as presented in Fig. 3. We first introduced our rationale to find decisive criteria for selecting the qualified traces that provide improved localization performance without prior environmental knowledge. Then, we proceeded with the processing steps to generate offline databases.

A. Inertial Data Selection

1) Rationale

When relying on pervasive resources to achieve a ubiquitous system, the characteristics of the collected data must be considered to evaluate and select trustworthy ones. With respect to inertial data selection, the principal concept behind the proposed scheme is as follows: In PDR-based methods, the horizontal attitude angles are measured under the assumption that external acceleration is absent, and walking acceleration is the only external acceleration source that acts on the device. However, when collecting inertial data from freely-moving users, external acceleration is prevalent owing to pedestrian behavior, walking speed, and the change in smartphone poses. Consequently, the attitude angles are susceptible to significant distortion that deforms the generated trace compared with the actual one.

In the early stages of data collection for a ubiquitous system, the correction of the collected traces is hindered by the absence of calibration resources (*i.e.*, floor plans or internal ANs). Therefore, the collected traces between the outer ANs (*i.e.*, GNSS or elevator ANs) should have a geometric shape nearly similar to the actual ones to achieve accurate localization performance after aligning them. To achieve geometric similarity (GS), the generated traces must preserve the actual shape with limited distortion in the measured angles and distances, regardless of the variation in scale and rotation of the entire trace (*i.e.*, that can be recovered by determining the transformation parameters).

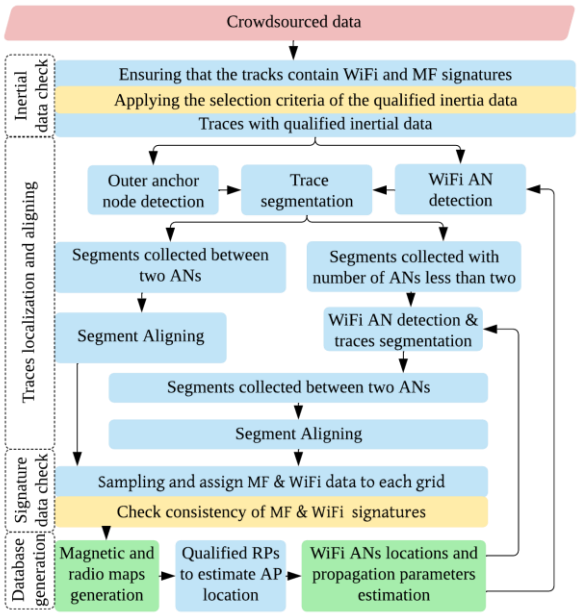

Fig. 3. The proposed scheme for offline database generation.

Notably, measuring the similarity between the collected and real traces is considered unfeasible without floor plans, as the case in developing ubiquitous systems. Consequently, the relationships between the GS and inertial data characteristics were tested to infer which data can reflect collecting traces with higher GS. These characteristics can distinguish qualified traces without any external requirements. An empirical test was conducted to determine these characteristics. The selection criteria were determined based on the results of the empirical analysis.

2) Empirical Test

We collected paths between two outer ANs (*i.e.*, installed inside two elevators, see Fig. 4 (a)) from different users, walking speeds, and smartphone poses. Five types of poses were considered, which included the users holding the smartphone horizontally, at their ear while calling, or in their swinging hand as they walked. The fourth pose involved the users keeping the smartphone in a front pocket. The fifth type of pose was a miscellaneous classification that included multiple poses. To measure the GS of the collected traces, we

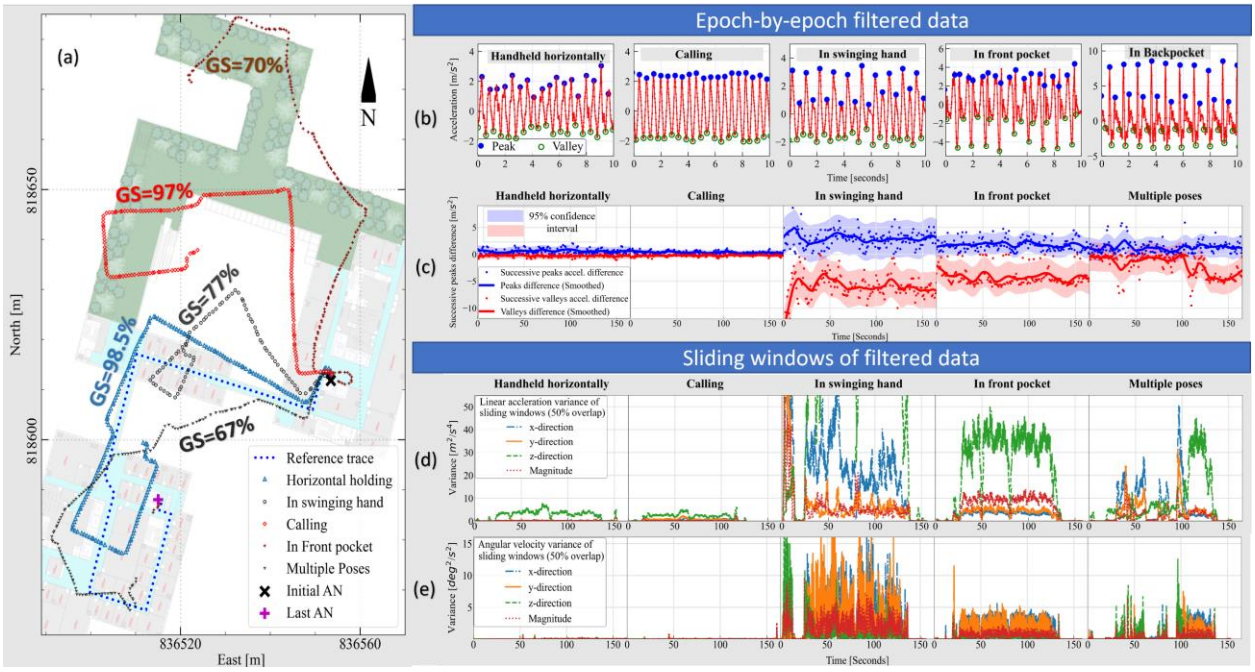

Fig. 4. (a) Geometric similarity (GS) of generated tracks based on PDR of different smartphone poses, (b) step peaks and valleys for different poses, (c) the differences between successive steps extremes, (d) variances of linear acceleration within sliding windows of 130 samples with 50% overlap, and (e) variances of angular velocity within sliding windows of 265 samples with 50% overlap.

used the building floor plan to extract the references of the generated traces. The generated trace was aligned by determining the transformation parameters (see Section IV.C). Subsequently, the RMSE of the aligned trace was calculated relative to that of the reference trace. Accordingly, the inertial data of the collected traces were analyzed to infer the characteristics that provide a high GS and low RMSE. GS measurement, data processing, and inferred criteria are discussed in the following subsections.

a) Measuring the GS

We employed a GS method that primarily reflects the preservation of trace shapes. The image-matching-based Hu moments method [31] was selected because it is invariant with rotation, transition, and scaling. The degree of similarity between the generated and reference traces was measured as follows: 1) the two traces were converted into two binary images with a similar scale and plotting area; 2) the seven Hu moments were computed (in-depth details can be found in [31]); subsequently a log transformation was applied to make them comparable; and 3) the GS between the generated and actual traces was computed as follows:

$$\mathrm{GS} = 100 - 100 \cdot \sum_{i=0}^{6} \left| \frac{m_i^r - m_i^g}{m_i^r} \right| \qquad (4)$$

where GS ranges from 0 to 100 and the top scores indicate a high GS. m_i^r and m_i^g are the i^{th} log-transformed Hu moments for actual and generated traces, respectively.

b) Inferring the Selection Criteria

The linear acceleration and angular velocity data for each trace were filtered using a low-pass filter to reflect pedestrian motion more clearly with less noise. The first feature was inferred from the filtered epoch-by-epoch acceleration data related to the acceleration differences between successive step extremes (peaks/valleys) (*i.e.*, obtained from the step detection results). These differences provided a distinct feature for the traces that provided a high degree of GS and low RMSE (see Fig. 5 (a)). When these differences were less than 3.0 m/s^2, the GSs were greater than 90%, and the average RMSE over the aligned traces was ~5.0 m. This was attributed to the low external acceleration attached to the walking acceleration when the differences between successive extremes were low. When carrying the smartphone in a stable position, such as horizontally handheld or calling, the extremes of the steps are formed with a nearly similar range of accelerations, as shown in Fig. 4 (b) and (c). The steady walking mode with a constant speed and the device carried in a stable pose could result in marginal differences between successive extremes, high GS, and low RMSE.

However, the differences in the extremes were the only remarkable feature obtained from the filtered epoch-by-epoch data; thus, a sliding window was applied to the filtered acceleration and angular velocity data with a 50% overlap to help extract more features. The statistical characteristics of the windows data were estimated relative to the x-, y-, and z-directions and their magnitudes. Among the different characteristics, the acceleration variances of the sliding windows provided remarkable features that distinguished traces with high GS and lower RMSE. Fig. 5 (b) shows the GSs and RMSEs estimated for the generated traces compared with the maximum acceleration variances recorded for their sliding windows. The traces that had sliding windows with maximum acceleration variances of less than 7 m^2/s^4 scored a GS higher than 90% and RMSE of 10.0 m. Thus, the maximum

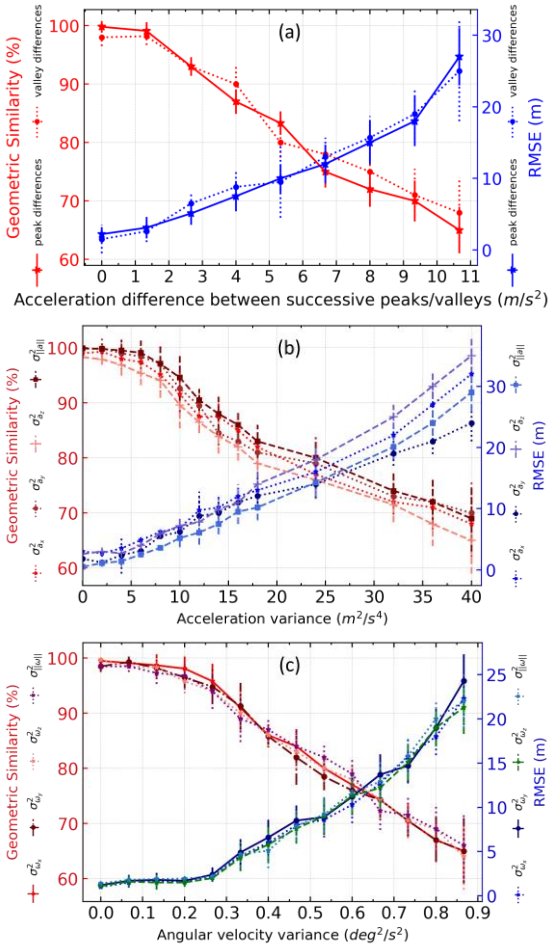

Fig. 5. Comparing the GS and RMSEs of the traces with (a) the acceleration differences between successive extremes, (b) the linear acceleration variances of the trace sliding windows, and (c) the angular velocity variances of the trace sliding windows.

acceleration variances of trace sliding windows can be considered another indicator of high GS. Notably, most of these traces were collected in handheld or calling poses. Similarly, the variance in the angular velocity provides another distinct feature. The higher GS and lower RMSE traces were characterized by maximum angular velocity variances lower than 0.25 deg^2/s^2. Fig. 5 (c) presents the GSs and RMSEs estimated for the generated traces compared with the angular velocity variances recorded for their sliding windows.

Based on the results of the empirical test, the inertial data of a portion of a trace were considered qualified if the following three criteria were satisfied: 1) the maximum differences between the successive peaks/valleys for the detected steps were less than 3.0 m/s^2; 2) the maximum acceleration variances (in x, y, z directions, and magnitude) of its sliding windows were less than 7 m^2/s^4; and 3) the maximum angular velocity variances (in x, y, z directions, and magnitude) of the sliding windows were less than 0.25 deg^2/s^2.

B. Outer Anchor Nodes Detection

In the initial stages of database generation, GNSS data with position accuracy higher than 5.0 m and horizontal dilution of precision (HDOP) less than 20 were considered qualified to serve as outer ANs to align the collected traces. With respect to elevator ANs, BLE RSS measurements are susceptible to large fluctuations (see Fig. 6). Therefore, an average filter was first applied to smooth the raw RSS data; subsequently, a sliding window was used to detect the RSS peak when the user traversed the beacon coverage area. Finally, when RSS peak exceeded a certain threshold, this ensured that the pedestrian was near the detected AN and the position of BLE AN (i.e., elevator location) was updated the user location.

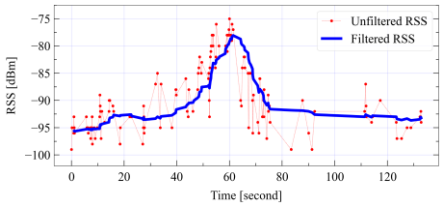

Fig. 6. BLE RSS smoothing and peak detection.

C. Traces Segmentation and Aligning

After identifying the number and locations of the detected outer ANs over portions with qualified inertial data, these portions were segmented into two types. The segments collected between two or more ANs were defined as closed segments. These segments were subsequently corrected and utilized to extract the database information in the initial stages. Conversely, segments that were located between less than two ANs were defined as open segments. These segments were corrected and utilized only after inferring information from the internal ANs (i.e., in subsequent generation stages).

The reference locations of the detected ANs that bound each closed segment were used to align the measured locations in this segment. This was accomplished by estimating the translation, rotation, and scaling parameters that minimized the RMSE of two sets of pairs (*i.e.*, the measured and reference locations of the ANs). Accordingly, for a closed segment with n ANs, the measured and reference locations of the ANs were defined as $\boldsymbol{B} = (\boldsymbol{b_1} \ldots . \boldsymbol{b_n})$ and $\boldsymbol{A} = (\boldsymbol{a_1} \ldots . \boldsymbol{a_n})$, respectively. The transformation parameters for aligning $\boldsymbol{B}$ with $\boldsymbol{A}$ were obtained using least-squares, as discussed in [32]. The demonstrated steps can be summarized as follows. First, the covariance matrix $\boldsymbol{H}$ and its singular value decomposition $\boldsymbol{UDV}$ were calculated as follows:

$$\boldsymbol{H} = \frac{1}{n}\sum_{i=0}^{n}\left(\boldsymbol{a}_i - \boldsymbol{\mu}_A\right)^T\left(\boldsymbol{b}_i - \boldsymbol{\mu}_B\right), \quad \boldsymbol{H} = \boldsymbol{UDV}^T \tag{5}$$

where $\boldsymbol{\mu}_A$ and $\boldsymbol{\mu}_B$ are the centroids of $\boldsymbol{A}$ and $\boldsymbol{B}$ points, respectively. Second, to detect and prevent reflections, the $\boldsymbol{S}$ matrix is computed as follows:

$$\boldsymbol{S} = diag\left(1, sgn\left(det\left(\boldsymbol{U}\right)det\left(\boldsymbol{V}^T\right)\right)\right) \tag{6}$$

where *sgn*, *det* and *diag* are the signum function, determinant, and diagonal matrix, respectively. Third, the optimal rotation matrix $\boldsymbol{R}$, scale factor s, and translation vector $\boldsymbol{t}$ are estimated as follows:

$$\boldsymbol{R} = \boldsymbol{U}\boldsymbol{S}\boldsymbol{V}^T, \quad s = \frac{\sigma_A^2}{\mathrm{tr}(\boldsymbol{D}\boldsymbol{S})}, \quad \boldsymbol{t} = \boldsymbol{\mu}_A - s\boldsymbol{R}\boldsymbol{\mu}_B \tag{7}$$

Finally, the aligned location $\boldsymbol{b}_i'$ for point i is estimated as $\boldsymbol{b}_i' = \boldsymbol{t} + s\boldsymbol{R}\boldsymbol{b}_i$. The aligned data for the selected traces were combined and spatially divided into small square grids of 0.5×0.5 m^2 and 1.0×1.0 m^2 to generate the magnetic and radio maps, respectively. Notably, the grids with a lack of steps (*i.e.*, less than 10% of the steps of the grid with the maximum number of steps) were filtered out to obtain dense signatures at the surviving grids. Finally, the quality of the signatures of the surviving grids was checked, as described in the following section.

D. Signature Data Selection

The quality of MF and RSS signatures of extracted grids was checked to ensure the quality of the clustered signatures at each grid as follows: (1) the WiFi APs with weak RSS (e.g., less than -90 dBm) were excluded; (2) at each grid, APs with few signatures (*e.g.*, less than a certain threshold) were discarded; (3) the grids with fewer than six unique APs were discarded, as recommended by [11], because the fingerprinting accuracy deteriorates when the number of APs was less than 6 per RP; (4) outlier filtering was conducted on the grids containing more data than the threshold. The RSS values for AP and MF data higher than $Q_3 + 1.5\,IQR$ or lower than $Q_1 - 1.5\,IQR$ were filtered out, where Q_1 and Q_3 are the 25th and 75th percentile values, respectively, and IQR indicates the interquartile range (*i.e.*, $Q_3 - Q_1$). The RP location was calculated as the coordinates of the grid center. In addition, the means of the RSS and MF data were calculated and assigned as a signature at the RP location. The surviving RPs created magnetic and radio maps. Moreover, these RPs were used to infer information from fixed WiFi APs that can serve as internal ANs within the floors, as discussed in the following subsection.

E. Fixed WiFi APs and Internal WiFi Anchor Nodes

1) Self-Identifying of the Fixed WiFi APs

Each time a crowdsourced dataset is collected, different WiFi APs may be observed, whether temporarily from mobile transmitters or permanently from fixed ones. Our scheme aims to self-identify the basic service set identifiers (BSSIDs) list of permanently observed and fixed APs to construct a radio map of the target floor. The construction of the radio map was confined to the observed fixed APs to reduce the computational overhead in the online positioning engine and improve the position estimation. A few considerations were made in selecting the fixed APs. First, frequently observed WiFi APs (*i.e.*, more than three days) were selected from the collected data. Subsequently, from the frequently observed APs, those with an RSS greater than -55 dBm were selected to ensure that the AP was within the target floor (*i.e.*, not observed from adjacent buildings, upper floors, or lower floors). In the following step, the AP strong signature locations were estimated from the aligned traces and clustered to ensure a WiFi AP is installed at a fixed location. Subsequently, the AP with a cluster area within 100 m^2 was considered a fixed AP. Finally, these fixed APs were used to construct the floor radio map.

2) Inferring Internal WiFi Anchor Nodes

Relying on only outer ANs to realize ubiquitous systems has the following limitations:1) long traces are susceptible to significant heading drift; 2) several traces with qualified inertial data may not be bounded by two outer ANs, and, therefore, cannot be included in the database; and 3) the generated databases cannot cover the entire floor area. Therefore, we aimed to infer the locations of fixed WiFi APs that can serve as internal ANs within the floor.

Thus, the locations of the fixed APs should be precisely estimated. We utilized the radio map generated from the closed segments aligned by the outer ANs to infer the qualified RPs. For each fixed AP, we checked the signatures of its RPs as follows:1) an RP was qualified to estimate the AP location if it contained dense signatures for this AP (*i.e.,* more than 20 from different traces) in combination with less signature variation (*i.e.*, $\sigma_{RSS} \leq 8$ dBm); 2) APs with qualified RPs (*i.e.,* more than 50) were only selected; and 3) the mean RSS of each qualified RPs was estimated to check if qualified RPs were observed with strong RSS (i.e., greater than -55 dBm).

If the qualified RPs for a fixed AP satisfied the aforementioned conditions, we considered it qualified to serve as AN, and its location (x_i, y_i), path-loss exponent (n_i), and RSS at 1 m ($rsso_i$) were estimated using the least-squares estimation method based on the path-loss propagation model [33] as follows:

$$\boldsymbol{rss}_{i,u} = -10n_i\, log_{10}\left(\sqrt{(x_i - \boldsymbol{x}_u)^2 - (y_i - \boldsymbol{y}_u)^2}\right) + rsso_i \tag{8}$$

where subscripts i and u indicate the fixed AN and the RP indices, respectively. The design matrix $\boldsymbol{D}_i$ is obtained as:

$$\boldsymbol{D}_i = \begin{bmatrix} \frac{-10n_i(x_i - x_{u,j})}{-10\,log_{10}\,d_{i,j}} & \frac{-10n_i(y_i - y_{u,j})}{-10\,log_{10}\,d_{i,j}} & -10\,log_{10}\,d_{i,j} & 1 \\ ..... & ..... & ..... & ..... \\ \frac{-10n_i(x_i - x_{u,N})}{-10\,log_{10}\,d_{i,N}} & \frac{-10n_i(y_i - y_{u,N})}{-10\,log_{10}\,d_{i,N}} & -10\,log_{10}\,d_{i,N} & 1 \end{bmatrix} \tag{9}$$

where j indicates the RP index and $d_{i,j} = 10^{\frac{rss_{i,j} - rsso_i}{10n_i}}$. The state vector $\hat{\boldsymbol{x}}_i = [x_i \;\; y_i \;\; n_i \;\; rsso_i]^T$, and covariance matrix $\hat{\boldsymbol{P}}_i$ are calculated as follows:

$$\begin{aligned} \hat{\boldsymbol{x}}_i &= (\boldsymbol{D}_i^T \boldsymbol{R}_i^{-1} \boldsymbol{D}_i)^T \boldsymbol{D}_i^T \boldsymbol{R}_i^{-1} \boldsymbol{z}_i \\ \hat{\boldsymbol{P}}_i &= (\boldsymbol{D}_i^T \boldsymbol{R}_i^{-1} \boldsymbol{D}_i)^{-1} \end{aligned} \tag{10}$$

where $\boldsymbol{z}_i$ is the observation vector (*i.e.*, equal to $\left[rss_1 \ldots rss_j \ldots rss_N\right]^T$), $\boldsymbol{R}_i = diag(\boldsymbol{\varepsilon}_{rssi})$ and $\boldsymbol{\varepsilon}_{rssi}$ is the RSS noise vector.

3) Aligning the Collected Traces Using the WiFi ANs

The following procedures were performed to use WiFi ANs to align the collected traces. The WiFi RSS data were smoothed using an average filter for each WiFi AN detected within trace data, and RSS peaks were determined. If the RSS of a peak was higher than or equal to the estimated $rsso$ for this AP, the location of this peak was considered as the measured AN location and added to the $\boldsymbol{B}$ vector (*i.e.*, that contains the measured locations of the detected ANs as stated in Section

IV.C). The estimated reference location for this AN was added to the $\boldsymbol{A}$ vector (*i.e.*, containing the reference locations of the detected ANs). Accordingly, these two vectors were used to determine the transformation parameters and align the trace.

V. Online Indoor Positioning

In our online scheme, the generated radio and magnetic maps were utilized to estimate fingerprinting solution; Section V.A illustrates the method of wireless localization-based fingerprinting. PDR was then integrated with the estimated fingerprinting solution using EKF to bridge wireless outages and curb PDR drift, refer to section V.B. Notably, before fusing fingerprinting and PDR solutions, the reliable relative PDR displacement and gyro heading change were leveraged to improve the selection of the best nearest neighboring RPs in certain scenarios.

A. Online Fingerprinting

In a conventional KWNN, selecting the best K neighboring RPs is based on the minimum summation of the Euclidean distance between the online MF and WiFi RSS signatures and the offline RPs. The online fingerprinting position $\boldsymbol{P}$ can then be estimated by:

$$\boldsymbol{P}=\left\{\sum_{i=1}^{\mathrm{K}}(x_i^{RP}\cdot w_i),\sum_{i=1}^{\mathrm{K}}(y_i^{RP}\cdot w_i)\right\} \tag{11}$$

where (x_i^{RP}, y_i^{RP}) is the position of i^{th} RP from the K-selected RPs and the weight w_i is computed as follows:

$$w_i=\frac{\frac{1}{(\xi_i)^2}}{\sum_{i=1}^{k}(1/\xi_i)^2} \tag{12}$$

where ξ is the difference between offline and online signatures. However, different locations possessing similar signatures exist. Moreover, the offline and online data vary [4, 19], especially when heterogeneous smartphones generate an offline database. Thus, selecting the best neighboring RPs may be susceptible to mismatching. To improve the selection of the best K neighboring RPs, we proposed utilizing the high credibility of the gyro heading change over short periods (*i.e.*, periods between two successive WiFi scans) and the accurate estimation of the walked distance and gyro heading during this period as aiding selection criteria. It is important to point out that this aiding can effectively exploited while the user is walking in straight line between successive WiFi scans. In these portions, the difference between the distance from each RP to the previous fingerprinting position and the PDR displacement between the two scans and the summation of gyro heading change should be equal zero.

Accordingly, to determine the selection criteria for the K-nearest RPs, walking status and λ_l were first estimated. If a WiFi scan was triggered during making a turn or while in a static mode, the K-nearest RPs were selected based on matching the MF and WiFi RSS signatures. Conversely, if a WiFi scan was triggered while the user was walking in a straight line (*i.e.*, $\Delta h_{max} \leq \lambda_l$, as stated in SectionIII), the distance walked and the heading change between the last WiFi scan were used to boost the selection of the K-nearest RPs. These approaches were applied as follows: We computed the distance from each RP to the previous fingerprinting position $(x_{t-1}^{FP}, y_{t-1}^{FP})$, and compared it with the distance walked within this period. The difference between the two distances $\xi_{\Delta d}$ is computed for each RP using the following expression:

$$\xi_{\Delta d}=\left|\sqrt{(x_i^{RP}-x_{t-1}^{FP})^2+(y_i^{RP}-y_{t-1}^{FP})^2}-\sum_{k=0}^{n}sl_k\right| \tag{13}$$

where n is the number of steps walked from the last WiFi scan (*t-1*), and *sl* is the estimated step length. The change in the heading ($\xi_{\Delta H}$) between two the straight lines was calculated. The first line was between the i^{th} RP and the preceding fingerprinting position and the second line was between the last two fingerprinting positions (*i.e.*, $(x_{t-1}^{FP}, y_{t-1}^{FP})$ and $(x_{t-2}^{FP}, y_{t-2}^{FP})$). The expression for $\xi_{\Delta H}$ is as follows:

$$\xi_{\Delta H}=\left|\arctan\left(\frac{y_i^{RP}-y_{t-1}^{FP}}{x_i^{RP}-x_{t-1}^{FP}}\right)-\arctan\left(\frac{y_{t-1}^{FP}-y_{t-2}^{FP}}{x_{t-1}^{FP}-x_{t-2}^{FP}}\right)\right| \tag{14}$$

When walking in a straight line, $\xi_{\Delta H}$ and $\xi_{\Delta d}$ should be equal to zero. Accordingly, the ξ_{RSS}, ξ_{MF}, $\xi_{\Delta d}$, and $\xi_{\Delta H}$ were summed, the K RPs with the least summation were selected as the K-nearest neighbors to the current user location, and the fingerprinting position was computed by weighting them.

B. Integrated Localization Based on Extended Kalman Filter

We proposed an integrated solution based on the EKF to combine the available measurements. The location of a pedestrian at timestamp t (x_t, y_t) is updated as soon as a new step is triggered, as follows:

$$\begin{cases} x_t = x_{t-1} + (1+s_t)\, d_t \sin(h_t) + \sigma_x \\ y_t = y_{t-1} + (1+s_t)\, d_t \cos(h_t) + \sigma_y \\ s_t = s_{t-1} + \sigma_s \\ h_t = h_{t-1} + \Delta h_t + \sigma_h \end{cases} \tag{15}$$

where d_t and s_t indicate the distance moved and distance correction, respectively. h_t and Δh_t are the heading and heading changes, respectively. σ_x, σ_y, σ_s and σ_h are the east, north, distance, and heading noises, respectively. In addition, owing to the nonlinearity of the PDR model, a nonlinear version of the Kalman filter (KF) was used [34]. The state vector is defined as $\boldsymbol{x} = [\delta_E \quad \delta_N \quad \delta_s \quad \delta_h]^T$, where δ is the error for each parameter. The transition model is linearized using a partial derivative. The state equation can be described as $\boldsymbol{x}_t = \boldsymbol{A}_{t-1,t}\boldsymbol{x}_{t-1} + \boldsymbol{B}\boldsymbol{\omega}_t$, where $\boldsymbol{A}_{t-1,t}$ indicates the state transition matrix from epoch $t-1$ to t, $\boldsymbol{B}$ is the system noise matrix, and $\boldsymbol{\omega}_t$ is the system noise vector with covariance matrix $\boldsymbol{Q}$: $\boldsymbol{\omega}_{t-1} \sim N(0, \boldsymbol{Q}_{t-1})$. Furthermore, because the error of the parameters within a small-time interval had a minimal value (*i.e.*, less than millimeters for the localization parameters), the higher-order term can be neglected. Thus, the transition matrix is expressed as:

$$\boldsymbol{A}=\begin{bmatrix} 1 & 0 & d_t\sin(h_t) & (1+s)\, d_t\cos(h_t) \\ 0 & 1 & d_t\cos(h_t) & (-1-s)\, d_t\sin(h_t) \\ 0 & 0 & 1 & 0 \\ 0 & 0 & 0 & 1 \end{bmatrix} \tag{16}$$

The observation mode can be represented as follows: $\boldsymbol{z}_t = \boldsymbol{C}_t\boldsymbol{x}_t + \boldsymbol{v}_t$, where $\boldsymbol{C}_t$ is the matrix used to estimate the predicted measurement $\boldsymbol{z}_t$ from the predicted state $\boldsymbol{x}_t$, and $\boldsymbol{v}_t$ is the observation noise which is assumed to have a zero mean with

the covariance matrix $\boldsymbol{R}$: $\boldsymbol{v}_t \sim \boldsymbol{N}(0, \boldsymbol{R}_t)$. The localization results from the inertial sensors and wireless measurements are incorporated into the observation vector as $\boldsymbol{z}_t = [\Delta E \quad \Delta N \quad \Delta s \quad \Delta h]^T$, where Δ is the bias in each parameter. The transition matrix $\boldsymbol{C}$ was defined as $diag(c_1, c_2, c_3, c_4)$ and covariance matrix $\boldsymbol{R}$ was donated as $diag(r_1, r_2, r_3, r_4)$.

When the WiFi scan was triggered, online position-based fingerprinting is estimated, the parameters c_1 and c_2 are set to 1. Δx and Δy are estimated as the difference between the PDR and fingerprinting positions and updated $\boldsymbol{z}$. The covariance matrix is updated as follows:

$$r_1 = r_2 = \sigma_{FP}^2 = \frac{\sum_{i=1}^{K}\left(w_i \cdot \sqrt{(x_{fp}-x_i)^2+(y_{fp}-y_i)^2}\right)}{\sum_{i=1}^{K}(w_i)} \quad (17)$$

where (x_{fp}, y_{fp}) is the estimated fingerprinting solution. (x_i, y_i) and w_i are the location and estimated weight of the i-th RP. K is the number of best neighboring RPs selected to estimate the fingerprinting position. When a user walks in a straight line between two ANs, the step length is calibrated as follows:

$$sl_{calib} = \frac{\hat{l}_{AB}}{N} = \frac{\sqrt{(dx_{AB})^2 + (dy_{AB})^2}}{N} \quad (18)$$

where $\hat{l}_{AB}$ is the actual distance between ANs A and B, dx_{AB} and dy_{AB} are the easting and northing between A and B, respectively, and N is the number of steps triggered between A and B. In the fusion model, the length parameters are updated as follows:

$$\Delta s = sl_{calib} - sl_{imp},\ c_3 = 1,\ and\ r_3 = 0.005 \quad (19)$$

where sl_{imp} is the estimated empirical step length. Similar to the step length calibration, the step heading is also calibrated after the user walks in a straight line between two ANs by computing the error in the estimated heading as follows:

$$h_\delta = \arctan\left(\frac{y_A^r - y_B^m}{x_A^r - x_B^m}\right) - \arctan\left(\frac{y_A^r - y_B^r}{x_A^r - x_B^r}\right) \quad (20)$$

where the superscripts m and r refer to the measured and reference locations of the detected ANs, in the EKF model. The heading parameters are updated as follows:

$$\Delta h = h_\delta,\ c_4 = 1,\ and\ r_4 = 0.001 \quad (21)$$

Then, the integrated position of the user is estimated as follows:

$$\begin{bmatrix} x_t \\ y_t \end{bmatrix} = \begin{bmatrix} x_{t-1} + \delta_x + (1 + s + \delta_s)\, d \sin(h + \delta_h) \\ y_{t-1} + \delta_y + (1 + s + \delta_s)\, d \cos(h + \delta_h) \end{bmatrix} \quad (22)$$

VI. Experiments, Results, and Evaluations

A. Experimental Settings

An Android application was developed to apply the proposed system to real-world scenarios. The developed application was written in JAVA code and was run entirely on smartphones. A Google Map API was used as the user interface to display the location of indoor pedestrians, as shown in Fig. 7. (a). The smartphones supported BLE and WiFi scans at intervals of 300 ms and ~3 s, respectively. For all the tests, the sampling frequency of the accelerometers and magnetometer was set to 50 Hz. A higher sampling frequency (*i.e.*, 100 Hz) was used for angular velocity measurements to accurately estimate the angular changes.

B. Tests Description and Setups

The tests can be broadly divided into 1) track-generation based on PDR, 2) offline database generation using crowdsourced data, and 3) online positioning. The setup and description of each test are presented below.

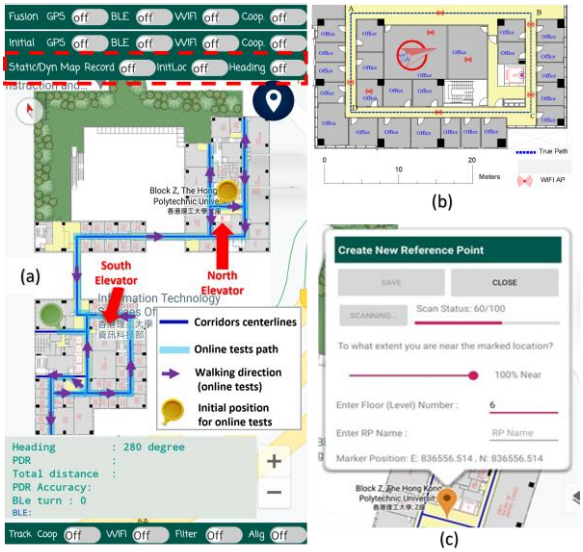

Fig. 7. (a) *Everywhere* user interface, (b) the pedometer test area, and (c) an interactive interface for checking the ground truth points and creating the manual fingerprinting databases.

1) Track Generation-based-PDR Tests

A rectangular corridor with a total length of 75.3 m, represented in Fig. 7 (b), was selected as a test field for step detection, length, and heading estimation. The total step count over the track is ~ 110 steps. Regarding step detection, experimenters walked along the corridor with different smartphone poses and three walking speeds (*i.e.*, slow, regular, and fast). Each experimenter manually counted the walked steps and recorded them as the actual steps count. We evaluated the step detection method by estimating the difference between the user count and the steps counted using the proposed approach. Additionally, we compared the detection accuracy of our approach with the mean crossing detection (MCD) method [27] and the fast Fourier transformation (FFT)-based peak detection method [35] for further evaluation of our method's performance.

The same track was walked ten times to assess the variation in step length estimation and heading performance over a long navigation period (~ 20 minutes). The step length was estimated using the nonlinear model and compared with: 1) the constant step length (*i.e.*, estimated as $sl = c \cdot h$, where h is the pedestrian height, and c is a constant equal to 0.413 and 0.415 for females and males, respectively), and 2) the linear model proposed in [36]. The heading from the gyroscope, MF, and calibrated weighted heading were estimated and compared with the reference heading. Finally, two tracks were used to evaluate the performance of turn detection and PDR outlier filtering. The results of each PDR part were demonstrated in Section VI.C.

2) Offline Database Generation Tests

Our test site was a large campus floor of ~7200 m^2, located on floor 6 of block Z, the Hong Kong Polytechnic University (see Fig. 11 (a)), comprising two blocks connected by two bridges and a garden. A BLE beacon was installed inside the north and south elevators (*i.e.,* the red arrows in Fig. 7 (a)). Floor users were invited to participate in the data collection after the assurance that their data would be protected. Most of those who accepted the invitation were willing to share their data in accessible, public, and authorized areas outside their offices and without accessing others' offices to avoid the COVID-19 pandemic. The volunteers were a group of students and colleagues with different body profiles, step lengths, walking behaviors, and models of Android smartphones. On average, there were seven volunteers per day. In terms of sex, there were approximately 3:4 women and men. Notably, no instructions were provided to them; they collected the data during their daily routines without altering their natural behaviors. The overall data were collected over 12 days at different times. The following data were recorded for offline database generation: raw inertial sensor measurements, WiFi scan information (*i.e.,* APs BSSIDs and RSS), BLE scan information (*i.e.,* UUID, minor ID, and RSS), GNSS data (*i.e.,* position, accuracy, and HDOP), MF readings, and the system timestamp of each measurement. The results of the generated database are presented in Section VI.D, and the database evaluation is presented in Section VI.E.

3) Online Positioning Tests

We designed three experiments to evaluate online positioning performance. A track with a total length of approximately 360 m extending from the north to the south block was used as the experimental field (see Fig. 7 (a)), and online data were collected using a smartphone carried in a horizontal handheld pose. The first test assessed the fingerprinting performance using different RP selection criteria. Next, the fingerprinting accuracy achieved using different types of databases was compared. Subsequently, the performance of the integrated solution based on EKF was evaluated, following which it was compared with PDR and fingerprinting solutions. The results of the three online tests are presented in Section VI.F.

4) Ground Truth, Static and Dynamic Database Establishment

The following setups were implemented to obtain ground truth points for evaluating the proposed system. The absolute locations of benchmarks were obtained in the garden area using Trimble R10 GNSS receiver. These benchmarks were equipped by Leica total station to obtain other benchmarks points within the floor. The floor benchmarks were employed to georeferenced digital map of the floor plan (*i.e.,* in AutoCAD format). The proposed method in [37] was conducted to create check points in online positioning tests by marking distinct features on the user interface screen. These features represented the reference position of the measured online location. Some key reasons for using the chosen method are its cost efficiency and the enriching of the floor plan with many distinct landmarks such as gates, corners, elevators, stairs, and office doors. By virtue of the georeferenced map, we labeled and estimated the absolute positions of floor landmarks (*i.e.,* distributed at distances approximately 6.0 m). Then, an interactive Google map-based marker labeling option (as shown in Fig. 7 (c)) was developed to facilitate recording the check points in online positioning experiments.

Static and dynamic database creation options were also included in the application interface for the testing purposes (*i.e.,* as can be shown from the red dashed rectangle in Fig. 7 (a)). Static RP was captured by dragging the developed Google map-based marker (*i.e.,* orange marker in Fig. 8 (c)) at the location of RP on the georeferenced map, then the WiFi and MF scans were recorded for 30 s using a Huawei Mate 20 Pro smartphone. A dynamic database was also created by walking each corridor separately at a constant walking speed. The position of each RP was estimated by interpolating between the walking steps.

C. Track Generation-based-PDR Results

TABLE II summarizes the statistical results of the step detection test. The overall performance of our proposed step detection method showed high accuracy for the handheld pose with a maximum detection error of less than 2%. Detection errors were also measured at different speeds, phone poses, and device models, and achieved mean and maximum error rates of 2.3% and 4.6% respectively. Additionally, the comparison with existing step detection methods (*i.e.,* MCD [27] and FFT [35]), see Fig. 9, verified that our proposed method can deliver similar performance with different smartphone poses. The statistical results of the step length estimation are summarized in TABLE III. The nonlinear step length model outperformed the linear model and the constant step length estimation methods, with a maximum error of 2 ± 1 m measured for a trajectory with a 75 m total length. The results of the heading estimation are visualized in Fig. 9. The MF heading scored a sharp variation with maximum error raised to 50º sometimes because of the indoor magnetic disturbance. The cumulative error of gyro heading reached 90º owing to the cumulative drift. However, the weighted heading achieved a higher accuracy with a maximum error of 5º after approximately 20 minutes of walking.

TABLE II
STEP DETECTION RESULTS

Activity	Speed	Error Percentage (%)					
		Mate 20 Pro		Huawei P20		Samsung Note 8	
		Mean	Max	Mean	Max	Mean	Max
Handheld	Slow	0.5	1.0	0.7	0.9	0.7	1.0
	Normal	0.3	0.5	0.5	0.8	0.6	1.2
	Fast	0.6	1.1	1.2	1.6	1.5	1.9
Calling	Slow	0.6	0.9	0.8	1.3	0.6	1.2
	Normal	0.3	0.6	0.4	0.8	0.5	1.0
	Fast	0.7	1.2	0.9	1.5	1.2	1.4
Swing	Slow	1.9	4.0	2.4	4.2	2.5	3.8
	Normal	1.8	3.2	2.0	3.0	2.1	3.1
	Fast	2.2	4.6	3.1	3.8	2.7	4.1
Pocket	Slow	1.2	2.0	1.5	2.3	1.3	2.0
	Normal	0.7	1.6	0.9	2.0	0.9	1.8
	Fast	1.5	2.2	1.4	3.1	1.6	2.5

Fig. 10 visualizes the localization performance of track generation-based-PDR method for two different tracks where the blue markers show the triggered turns. Fig. 10 (a) shows the steps utilized to initialize the RANSAC model after each turn (*i.e.*, plotted by a black line). Fig. 10 (b) visualized the linear model estimated using RANSAC to filter PDR outliers (i.e., plotted by the red lines). The proposed model successfully detected all the turns and accurately localized the triggered steps with outliers less than 0.75 m (compared to the centerlines positions of the corridors).

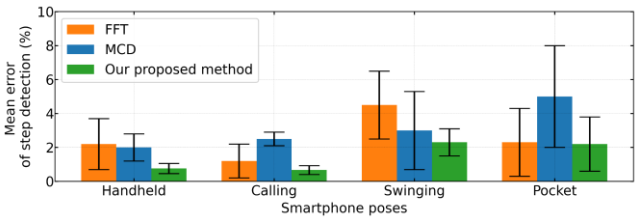

Fig. 8. Performance comparison of different step detection methods.

TABLE III
STEP LENGTH ESTIMATION RESULTS

Model	Error in meters					
	Mate 20 Pro		Huawei P20		Samsung Note 8	
	Std m (%)	Max m (%)	Std m (%)	Max m (%)	Std m (%)	Max m (%)
Constant	1.2(1.6)	1.9(2.5)	1.4(1.8)	2.7(3.6)	1.3(1.7)	2.5(3.3)
Linear	1.3(1.7)	2.2(2.9)	1.2(1.6)	2.9(3.8)	1.5(2.0)	3.7(4.9)
Non-linear	0.5(0.7)	1.6(2.1)	0.4(0.5)	1.9(2.5)	0.8(1.1)	1.5(2.0)

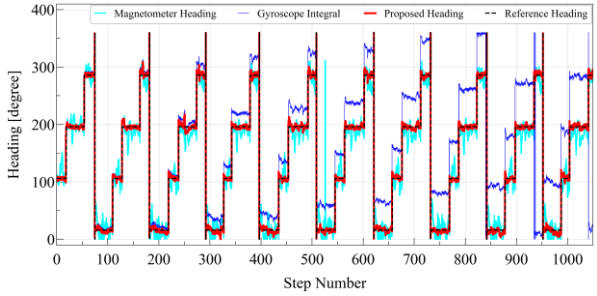

Fig. 9. Performance comparison of different heading estimation methods.

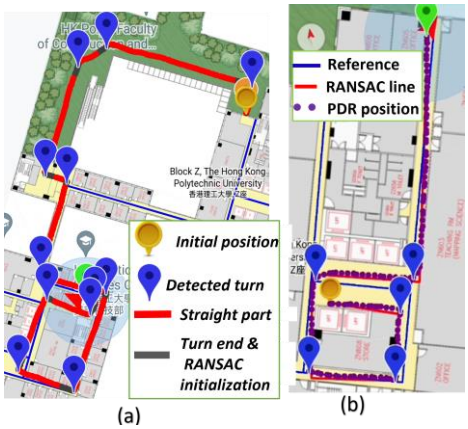

Fig. 10. Performance of turn detection, outlier filtering, and PDR localization.

D. Offline Database Generation Results

More than 249 tracks were collected within 12 days. Fig. 11 (a) shows the floor plan of the test area, and Fig. 11 (b) displays the generated tracks of all collected traces before handling. We first applied the preprocessing steps prior to the application of the inertial data selection criteria as follows:1) our proposed step detection procedures were employed to detect the triggered steps and estimate the accelerations at the step peaks and valleys; and 2) a sliding window with 50% overlap was applied to the filtered linear acceleration and angular velocities with sample sizes of 130 and 265, respectively. The selection criteria of the inertial data (see Section IV.A) were applied to all collected traces. The portions of tracks that satisfied these criteria were considered to contribute to database generation, whereas the others were discarded. Table IV illustrates the number of collected data and the percentage of the unqualified and qualified portions. The tracks generated from the qualified inertial data before aligning their positions are presented in Fig. 11 (c). TABLE IV summarizes the statistical properties of the selected inertial data characteristics of the qualified portions.

1) Initial Generation

In the initial generation, the outer ANs that satisfied the ANs conditions (see Section IV.B) were used to align the collected portions with the qualified inertial data. Table IV shows the percentage of closed and opened segments, where the mean percentage of closed segments was approximately 20% of the qualified portions. The closed segments were aligned by determining the optimal transformation parameters (Section IV.C). Fig. 12 (a) shows the localization solution of the samples of closed traces before and after aligning them. Fig. 12 (b) shows the alignment of the entire closed segment by the outer ANs. All the aligned portions were combined, and the entire covered area was divided into small grids with a size 1.0 m^2 to generate the grids of the radio map. About 2738 grids were obtained in at least one step. However, only grids with more than four steps were considered when generating the floor map. Fig. 12 (c) shows the remaining grids (only 661 grids) after filtering, indicating the presence of areas that are not covered by dense data and , consequently, excluded from the generated map.

Subsequently, the BSSIDs of the fixed and permanent WiFi APs were identified to construct the radio map of the target floor. Table IV shows that the mean number of WiFi APs is approximately 400 per day. Only 32 APs out of 400 were detected several times per day for more than three days and were considered permanent APs. The locations of signatures stronger than -65 dBm for the 32 APs were obtained from the aligned data. To better distinguish the APs installed in a fixed position, only the APs with signatures' locations clustered in less than 100 m^2 we selected. Of the 32 APs, 25 satisfied the last condition and were considered to be installed at fixed locations, and their BSSIDs were used to construct the floor radio map. Of the 25 APs, eight had qualified RPs data to estimate their APs locations after checking the stated conditions in Section (IV.E.2). Fig. 13 shows the qualified RPs of WiFi ANs for three of the eight WiFi ANs. The location and propagation parameters were then estimated for the eight WiFi

TABLE V
CROWDSOURCED DATA PROCESSING WITH TIME

Days	Number of tracks	Inertial data check		Total detected WiFi APs[1]	Fixed and permanent observed APs[2]	Segments with outer ANs		Number of internal WiFi ANs[3]	After inferring the locations of 8 WiFi APs to act as internal ANs	Open segments converted to closed[4]
		Unqualified portions	Qualified portions			< 2 Open	≥ 2 Closed			
Day 1 & 2	29	31%	69%	409	-	91%	8%	-		71%
Day 3 & 4	38	55%	45%	487	-	72%	28%	-		52%
Day 5 & 6	54	68.5%	30.5%	464	22	84%	16%	-		63%
Day 7 & 8	43	65%	35%	505	23	76%	24%	3		72%
Day 9 & 10	45	73%	27%	393	25	78%	22%	6		69%
Day 11&12	40	52.5%	47.5%	532	25	81%	19%	8		67%

[1]Mean number of APs per day, [2]The BSSIDs of the fixed WiFi APs used for radio map generation (cumulatively counted); [3]the WiFi APs with RPs qualified to estimate their positions to act as ANs (cumulatively counted); [4] a percentage from the open portions.

ANs, as described in Section (IV.E.2). The estimated locations of the WiFi ANs were compared with their actual locations. The mean and maximum RMSEs were approximately 1.12 m and 1.91 m, respectively. Finally, the reference RSS (*i.e.*, at 1.0 m) and loss exponent were estimated for the eight WiFi ANs (see Fig. 13).

TABLE IV
STATISTICAL SUMMARY OF THE INERTIAL DATA CHARACTERISTICS OF THE QUALIFIED PORTIONS

	Mean	**Std.**	**Min.**	**25%**	**50%**	**75%**	**Max.**
σ_{ax}	1.16	0.66	0.23	0.72	1.01	1.40	3.61
σ_{ay}	1.22	0.83	0.31	0.67	1.03	1.49	4.76
σ_{az}	2.70	1.35	0.77	1.69	2.36	3.45	6.88
$\sigma_{\|\|a\|\|}$	1.24	0.89	0.38	0.65	0.89	1.51	4.71
$\sigma_{\omega x}$	0.06	0.04	0.02	0.04	0.05	0.07	0.28
$\sigma_{\omega y}$	0.04	0.03	0.01	0.02	0.04	0.05	0.19
$\sigma_{\omega z}$	0.05	0.03	0.01	0.03	0.04	0.06	0.20
$\sigma_{\|\|\omega\|\|}$	0.04	0.02	0.01	0.03	0.04	0.05	0.16
Δ_{Peak}	1.82	0.57	0.51	1.41	1.85	2.15	2.90
Δ_{Valley}	1.39	0.57	0.38	0.99	1.29	1.71	2.85

2) Subsequent Generation

In the second generation, the inferred WiFi ANs were leveraged to align the segments with qualified inertial data, as described in Section (IV.E.3). Samples of trace alignment using WiFi ANs and outer ANs are shown in Fig. 14 (a). The upper-right panel in Fig. 14 (a) shows a remarkable enhancement in aligning the open trace. Additionally, aligning the traces with outer ANs together with WiFi ANs improved the alignment even for the closed segments, as shown in the upper left panel. By virtue of the inferred WiFi ANs, up to 70% of the open segments were converted into closed segments (see Table IV). Fig. 14 (b) displays the localization of all aligned traces by internal and outer ANs. Fig. 14 (c) shows the grids generated after combining the aligned traces, reflecting the extension of the spatial coverage of the generated map. The generated grids were then used to create magnetic and radio-map RPs.

The clustered signatures at each grid were checked to ensure consistency of the RPs using the criteria stated in Section IV.D. Fig. 15 shows the radio maps generated for nine out of the 25 fixed WiFi APs. Notably, the displayed RPs satisfied the signature quality check, and the total number of these RPs is attached to each plot. Fig. 15 shows that the reference location of the WiFi AP almost coincides with the location of the strong signature. Fig. 16 (a) shows the magnetic field measurements over the aligned traces, and Fig. 16 (b) shows the generated magnetic map.

3) Database Generation Over Time

Developing a generated database over time is crucial for developing a self-deployable system. Without dependency on floor plans, user feedback, or internal BLE ANs in the initial generation stage, only traces entirely collected with qualified data between outer ANs were considered for the database regardless of their lengths. At this stage, the following points are worth mentioning:1) as shown in Table IV, several traces with qualified inertial data (~80%) did not contribute to database generation because of their locations lacked calibration resources; 2) the spatial coverage of the initial database was confined to the common paths between outer ANs, as shown in Fig. 13 (c); and 3) long traces were exposed to heading drift owing to the long walking paths between the outer ANs and the absence of internal ANs in such a large-scale building, as shown in Fig. 13 (b). Inferring pervasive adjustment resources is a feasible solution for extending the spatial coverage and overcoming heading drift.

The cumulative increase in data over time improved the probability of obtaining more traces with qualified inertial data between the outer ANs, which, in turn, helped increase the number of qualified RPs to infer the locations of internal WiFi APs. For example, from Table IV, by day seven, the RPs data for only three fixed WiFi APs were qualified to estimate their APs positions. The number of ANs increased over time, and reaching eight APs by day 12. Hence, we can conclude that as time progresses, more fixed WiFi APs can be expected to obtain qualified RPs to estimate their locations. Deriving the locations of WiFi APs to serve as internal ANs significantly increases the quantity of contributed data, which can explain why the frequency of user movements within the floor areas is higher than that when the users cross from the outdoors to the indoors, or vice versa. Most of the open segments generated from traces within the floor were boosted by internal WiFi ANs and converted into closed segments, aligned, and included in the database. Accordingly, the spatial coverage of the next generated databases was extended to zones far away from the common paths between the floor entrances, as shown in Fig. 14 (c). In summary, we can conclude that cumulative increase in the amount of data is beneficial for developing a ubiquitous system. Moreover, updating the database with time can keep the database pace with frequent changes in WiFi APs.

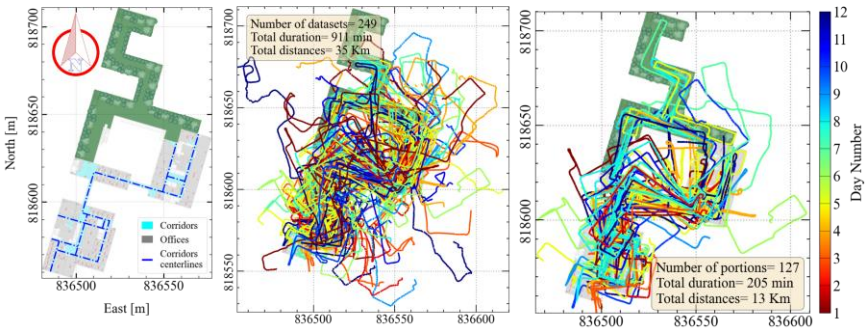

Fig. 11. (a) The sixth-floor plan, (b) the track generation of the entire collected data, and (c) the track generation of the portions with qualified inertial data.

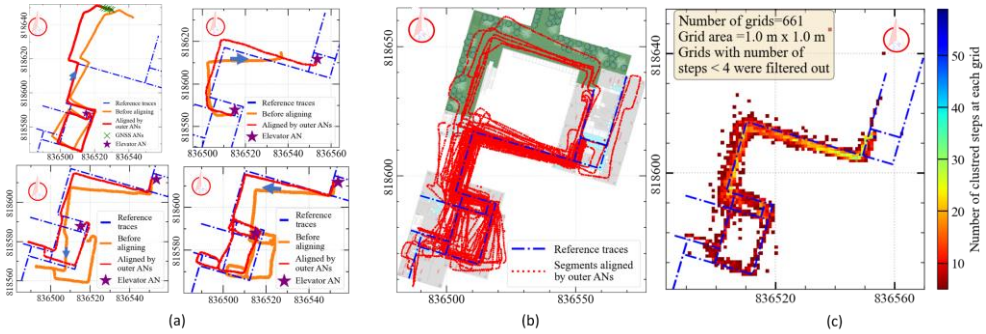

Fig. 12. (a) Samples of traces aligned by outer ANs, (b) the closed traces aligned by outer ANs, and (c) the generated grids from the aligned traces obtained from (b) to create the radio map at the initial generation stage.

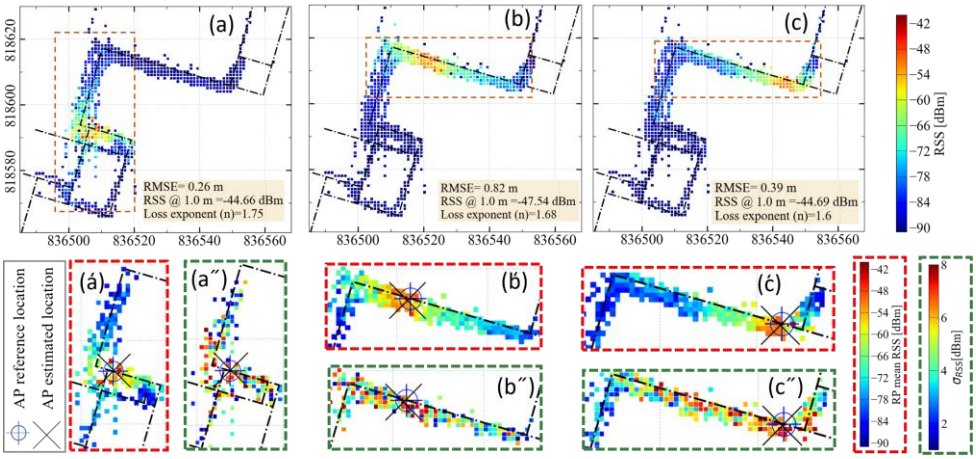

Fig. 13. Radio map for WiFi ANs from the initial generation stage. (a), (b), and (c) represent the radio maps for three selected WiFi APs. (a′), (b′) and (c′) display the mean RSS of the qualified RPs used to estimate the location information of the three WiFi ANs (panels and color bar are bounded by red dashed rectangle). (a″), (b″), and (c″) show the standard deviation of the RSS values of the qualified RPs (panels and color bar are bounded by green dashed rectangle).

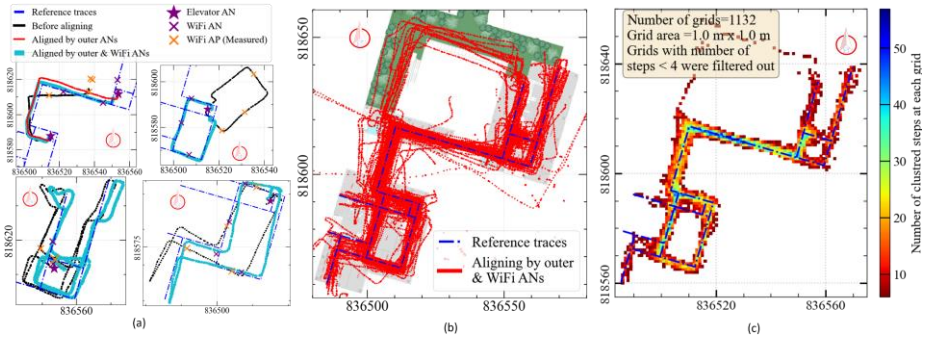

Fig. 14. (a) Samples of traces aligned by outer and internal WiFi ANs, (b) the alignment of the whole traces with qualified inertial data aligned by outer or internal WiFi ANs, and (c) the generated grids to create the radio map at the second-generation stage.

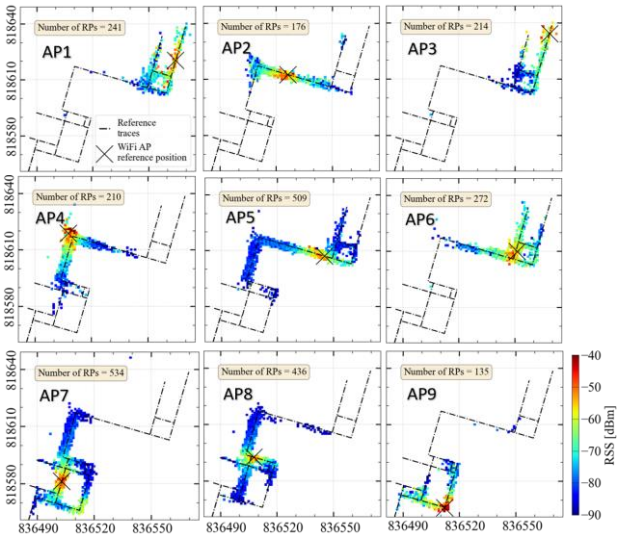

Fig. 15. The second-generation of the radio maps for 9 APs out of the 25 fixed WiFi APs (RPs satisfied the signature quality check are plotted, whereas the other RPs were set to -100 dBm and not visualized here).

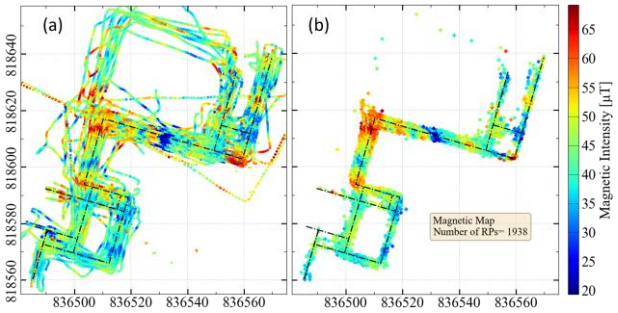

Fig. 16. (a) the MF over the aligned traces, and (b) the second-generation of the magnetic map (RP area 0.5×0.5 m^2).

E. Evaluation of the Crowdsourced Databases

We considered the database created by static surveying to be the most trustworthy for assessing the signatures of crowdsourced databases. Consequently, we compared the second generated crowdsourced radio and magnetic maps (*i.e.*, presented in Fig. 15 and Fig. 16 (b)) with the corresponding static maps. For the radio map, the absolute difference between the RSS of the crowdsourced RPs and the corresponding RSS of the static RPs was calculated for each fixed WiFi AP. A similar comparison was performed for the magnetic map, where the mean magnetic norm of each crowdsourced RP was compared with the corresponding static RP norm. Table VI summarizes the differences between the maps. The RSS differences scored a mean difference of approximately 6 dBm, and 75% of the results were less than 9.5 dBm. Similarly, the mean MF differences was approximately 5 μT, and 75% of the results were less than 6.7 μT.

Particularly, the validation was mainly executed to investigate the extent to which the crowdsourced signatures differed from the static signatures (i.e., the most trusted RPs). Notably, these differences were expected to occur and can be ascribed to the variability of the crowdsourced signatures collected by free-moving users who carried heterogeneous smartphones, whereas the human-supervised static databases were created in static mode at the actual locations of their RPs. However, the positioning results of crowdsourced databases are the predominant factor in the final decision on whether the proposed method is applicable in real localization scenarios.

TABLE VI
DIFFERENCES BETWEEN THE CROWDSOURCED AND STATIC SURVEYING SIGNATURES

	Mean	Std.	25%	50%	75%	90%
WiFi RSS (dBm)	6.1	4.8	2.4	5.2	9.5	12.3
MF (μT)	5.2	3.1	1.8	4.9	6.7	7.2

F. Online Positioning Results

1) Fingerprinting Performance Using Different Selection Criteria for the K-Nearest RPs

Using the same online dataset, we compared the online fingerprinting results when the K-nearest RPs were selected based on the RSS only, (RSS and MF), and (RSS, MF, and PDR displacement and orientation change). The second generation of crowdsourced databases (*i.e.*, presented in Fig. 15 and Fig. 16 (b)) was utilized to test the three selection criteria. The test was conducted on the designed online testing path shown in Fig. 7 (a). Fig. 17 (a) shows the empirical cumulative distribution function (ECDF) of the localization error for the three selection criteria. The combination of RSS, MF, and PDR provided localization errors of ~ 75% below 2.95 m with a mean error of 2.05 m. In contrast, the RSS and (RSS & MF) scored 75% of the errors of 3.35 and 3.5 m with a mean error of 2.55 and 2.4 m, respectively. Therefore, we can conclude that the accuracy is enhanced by approximately 18% when PDR guides the selection of the best K-nearest RPs, together with both RSS and MF signatures.

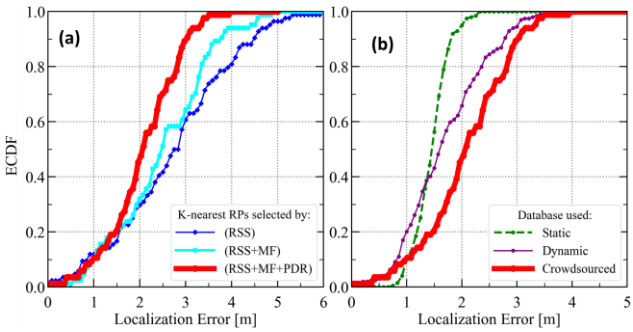

Fig. 17. ECDF of fingerprinting results using (a) different K-nearest RPs selection criteria and (b) different database creation techniques.

2) Fingerprinting Performance Using Different Creation methods for the Offline Databases

In the next step, we used the same online dataset utilized in the previous test and the selection of the K-nearest RPs based on the RSS, MF, and PDR changes in displacement and

orientation. Using these, we altered the crowdsourced databases to static surveying and dynamic walking databases to estimate the fingerprinting solution for each database type. Fig. 17 (b) shows the ECDF results for each database type. The positioning results indicate that the static database achieved the best accuracy compared to dynamic walking and crowdsourced database with a mean and 90% of the localization errors of 1.5 m and 2.0 m, respectively. However, the crowdsourced databases achieved a mean error of 2.1 m, and 90% of the localization errors were less than 3.5 m.

3) PDR, Fingerprinting, and EKF Results

This test compared the online solutions-based PDR, fingerprinting, and EKF methods. We used the second generated crowdsourced database as the offline database and selected the K-nearest RPs based on the combination of (RSS, MF, and PDR) for online matching. The EKF results outperformed PDR and fingerprinting solutions with a mean error of ~1.42 m compared with 1.83 m and 2.05 m for PDR and fingerprinting solutions, respectively. TABLE VII lists the accuracy achieved for each method and Fig. 19 shows the positioning solution for each method.

G. Comparison with Existing Approaches

We compared our proposed framework with existing counterparts in terms of the capability of developing ubiquitous systems and solution accuracy, as listed in TABLE VIII. The SoiCP system [17] achieves a positioning accuracy of 3.0 m and depends on accurate GNSS data to align the collected traces. Although SoiCP can attain a certain level of ubiquity with buildings surrounded by open-sky areas, it performs badly when applied to multistory buildings. Moreover, its accuracy would deteriorate even further when employed for buildings surrounded by GNSS-denied areas. The 3D-CSWS system [11] deployed six BLE internal ANs and achieved an accuracy of 1.98 m and 5.18 m in the office and the open areas, respectively; similarly, ten BLE ANs were deployed per floor in [10] that provided positioning accuracy of about 6.3 m. Similarly, [16] deployed BLE beacons at intervals of 7.0 m. We also collected crowdsourced data after deploying four internal BLE ANs to practically compare the performance of two cases: 1) with outer ANs only (i.e., as proposed in our scheme); and 2) with the existence of internal ANs (i.e., as proposed in existing work). In the second case, less total time was required to collect massive qualified closed traces between ANs data and generate the final databases. Also, better aligning for the collected traces with less heading drift was achieved owing to the availability of short paths between internal ANs. The database generated from the second case achieved a marginal fingerprinting accuracy improvement (less than 5%) compared with that obtained from the database of the first case. However, in multistory and large-scale buildings, a large number of BLE beacons are required to satisfy the requirements of such systems, which is costly and labor-intensive. Consequently, the ubiquity of these systems (i.e., that require internal auxiliary ANs) is limited and the accuracy improvement is marginal.

TABLE VII
PDR, FINGERPRINTING, AND EKF SOLUTIONS ACCURACIES

Solution	Mean	Max	75%	90%
PDR	1.83	7.70	3.20	4.30
Fingerprinting	2.10	5.40	2.80	3.50
EKF	1.42	6.30	2.35	3.15

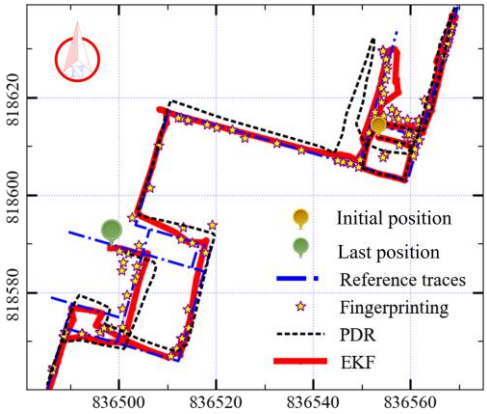

Fig. 18. Localization results of PDR, fingerprinting, and EKF.

TABLE VIII
COMPARISON WITH EXISTING SYSTEMS

System	Cost and effort	Suitable for building surrounded by		Accuracy
		GNSS-denied area	Open-sky area	
3D-CSWS [11]	Costly and tedious	✓	✓	1.9 m
[16]	Costly and tedious	✓	✓	1.0 m
[10]	Costly and tedious	✓	✓	6.3 m
SoiCP [17]	Low-cost and applicable	✗	✓	3.0 m
Everywhere	Low-cost and applicable	✓	✓	2.1 m

Our system, similar to SoiCP, leverages the available GNSS accurate data to serve as outer ANs and deploys an outer BLE AN inside the building's elevator. Thereby, it guarantees accurate localization even for the building surrounded by GNSS-denied areas, where one node can precisely serve as outer AN for all floors and saves the cost of deploying dense internal ANs at each floor. Thus, the proposed system can guide the development of ubiquitous systems. Additionally, the accuracy of our fingerprinting solution is superior to that of its counterparts by the virtue of the quality of the generated offline database and the improved selection criteria of the neighboring RPs in the online stage.

VII. CONCLUSION AND FUTURE WORK

The widespread use of smartphones and their unlimited spatial coverage of human mobility have enabled the collection of pervasive crowdsourced signatures. Consequently, autonomous localization of such signatures can be used to develop a self-deployable and ubiquitous IPS. However, previous indoor positioning studies-based crowdsourcing have not paid attention to the overarching aim of utilizing such data.

The sources and methods used in these studies potentially militate against realizing ubiquitous systems. The proposed framework relies on multisensory integration to develop a low-cost, self-deployable, and ubiquitous IPS that can be used for buildings surrounded by either GNSS-denied or open-sky areas. Compared with existing crowdsourcing-indoor positioning systems, our system has the following contributions:

1. In the offline phase, we introduced selection criteria for qualified inertial data that depended entirely on the characteristics of the collected data and eliminated the need for external resources. These criteria helped to include the data that generated traces with a geometric shape similar to the ones that are actually described by users. Including only traces with qualified data helped achieve better trace localization after aligning them and consistent signatures per RP after combining them (i.e., with mean differences less than 6 dBm and 5 μT, for the radio and magnetic signatures, respectively, compared to the reference signature-based static surveying).
2. Additionally, we reduced the expected large errors while depending on GNSS ANs to localize crowdsourced signatures in buildings surrounded by GNSS-denied areas or those with multiple stories by deploying BLE AN per elevator. The deployment of BLE beacons facilitates the maintenance of a high localization accuracy with low cost and effort.
3. Furthermore, to improve trace localization and extend the spatial coverage of the generated databases without the need to deploy BLE ANs within the floors or utilize floor plans, we leveraged the phenomenon of cumulative data densification to derive the identifiers, locations, and propagation information of fixed WiFi APs that can serve act as internal ANs. The estimated locations of the inferred WiFi ANs achieved mean and maximum RMSEs of approximately 1.12 m and 1.91 m, respectively. These inferred pervasive ANs significantly extended the spatial coverage and improved trace localization in subsequent database generation.
4. In the online phase, we exploited the high credibility of the short-period gyro heading change and PDR displacement to boost the selection of the best K-nearest RPs. This enhanced online fingerprinting by approximately 18%, with a mean accuracy of 2.1 m. Our integrated solution achieved a mean and 90% accuracy of about 1.42 m and 3.15 m, respectively. Interestingly, our system outperformed its counterparts and promoted ubiquitous IPS development for buildings surrounded by either open-sky or GNSS-denied areas.

Because the research on ubiquitous indoor localization is at an early stage, more improvements are probably required. However, the concepts introduced in this study should help guide research in this area. Here, we shed light on further improvements and considerations that could extend our work in developing ubiquitous IPSs, as follows: 1) utilizing other pervasive features to augment the adjustment of trace localization; 2) including barometric data and elevator acceleration patterns to obtain 3D indoor localization; 3) introducing attitude estimation approaches to improve the overall PDR performance in online navigation with different smartphone poses (*e.g.*, calling, swinging, in-pocket, and in-handbag poses); and 4) examining online fingerprinting performance in open-space areas.

Using the proposed system, regular users can easily produce the requirements of IPSs (i.e., that limit the ubiquity of IPSs). If such crowdsourcing systems are widely deployed, LBSs can ubiquitously improve their accuracy indoors. It is, however, crucial to propose user-friendly data collection strategies and privacy guarantees in order to make such promising systems widely adopted. Ignoring the negative impact of data collection on the users' devices (e.g., battery power draining and device performance slowing) can limit the applicability and widespread of the crowdsourced-IPSs. Therefore, protecting user data privacy and reducing the cost borne by the user device to collect these data must be seriously considered.

ACKNOWLEDGMENT

The authors would like to thank all the volunteers who collected the experiments data. The authors wish to thank the anonymous reviewers for their valuable comments.

REFERENCES

[1] P. Uphaus, B. Beringer, K. Siemens, A. Ehlers, and H. Rau, "Location-based services–the market: success factors and emerging trends from an exploratory approach," *J Locat Based Serv*, vol. 15, no. 1, pp. 1-26, 2021.

[2] A. M. Senousi, J. Zhang, W. Shi, and X. Liu, "A Proposed Framework for Identification of Indicators to Model High-Frequency Cities," *Isprs Int J Geo-Inf*, vol. 10, no. 5, p. 317, 2021.

[3] F. Furfari *et al.*, "Discovering location based services: A unified approach for heterogeneous indoor localization systems," *Internet of Things*, vol. 13, p. 100334, 2021/03/01/ 2021.

[4] X. Zhou, T. Chen, D. Guo, X. Teng, and B. Yuan, "From one to crowd: a survey on crowdsourcing-based wireless indoor localization," *Frontiers of Computer Science*, vol. 12, no. 3, pp. 423-450, 2018/06/01 2018.

[5] J. Ye, Y. Li, H. Luo, J. Wang, W. Chen, and Q. Zhang, "Hybrid Urban Canyon Pedestrian Navigation Scheme Combined PDR, GNSS and Beacon Based on Smartphone," *Remote Sensing*, vol. 11, no. 18, 2019.

[6] X. Zhu, W. Qu, T. Qiu, L. Zhao, M. Atiquzzaman, and D. O. Wu, "Indoor Intelligent Fingerprint-Based Localization: Principles, Approaches and Challenges," *IEEE Communications Surveys & Tutorials*, vol. 22, no. 4, pp. 2634-2657, 2020.

[7] A. Rai, K. K. Chintalapudi, V. N. Padmanabhan, and R. Sen, "Zee: Zero-effort crowdsourcing for indoor localization," 2012, pp. 293-304

[8] H. LUO, D. WENG, and W. CHEN, "An Improved Shadow Matching Method for Smartphone Positioning," *Geomatics and Information Science of Wuhan University*, vol. 46, no. 12, pp. 1907-1915, 2021.

[9] Y. Li, Z. He, Z. Gao, Y. Zhuang, C. Shi, and N. El-Sheimy, "Toward Robust Crowdsourcing-Based Localization: A Fingerprinting Accuracy Indicator Enhanced Wireless/Magnetic/Inertial Integration Approach," *IEEE Internet of Things Journal*, vol. 6, no. 2, pp. 3585-3600, 2019.

[10] P. Zhang *et al.*, "A Localization Database Establishment Method Based on Crowdsourcing Inertial Sensor Data and Quality Assessment Criteria," *IEEE Internet of Things Journal*, vol. 5, no. 6, pp. 4764-4777, 2018.

[11] Y. Yu, R. Chen, L. Chen, W. Li, Y. Wu, and H. Zhou, "Autonomous 3D Indoor Localization Based on Crowdsourced Wi-Fi Fingerprinting And MEMS Sensors," *Ieee Sens J*, pp. 1-1, 2021.

[12] C. Lee, Y. Kim, and K. Kim, "Clustering-assisted Stacked Generalization Approach for Fingerprint Crowdsourcing-based Indoor Localization," *Proceedings of the Korean Information Science Society Conference*, pp. 663-664, 2020.

[13] E. S. Lohan, J. Torres-Sospedra, H. Leppäkoski, P. Richter, Z. Peng, and J. Huerta, "Wi-Fi Crowdsourced Fingerprinting Dataset for Indoor Positioning," *Data*, vol. 2, no. 4, p. 32, 2017.

[14] R. Santos *et al.*, "Crowdsourcing-Based Fingerprinting for Indoor Location in Multi-Storey Buildings," *Ieee Access*, vol. 9, pp. 31143-31160, 2021.

[15] F. Q. Gu, S. Valaee, K. Khoshelham, J. G. Shang, and R. Zhang, "Landmark Graph-Based Indoor Localization," (in English), *Ieee Internet of Things Journal*, vol. 7, no. 9, pp. 8343-8355, Sept 2020.

[16] Y. Yu *et al.*, "A Novel 3D Indoor Localization Algorithm Based on BLE and Multiple Sensors," *IEEE Internet of Things Journal*, pp. 1-1, 2021.

[17] Z. Li, X. H. Zhao, F. Y. Hu, Z. L. Zhao, J. L. C. Villacres, and T. Braun, "SoiCP: A Seamless Outdoor-Indoor Crowdsensing Positioning System," (in English), *Ieee Internet of Things Journal*, vol. 6, no. 5, pp. 8626-8644, Oct 2019.

[18] J. Ye, X. Li, X. Zhang, Q. Zhang, and W. Chen, "Deep learning-based human activity real-time recognition for pedestrian navigation," *Sensors-Basel*, vol. 20, no. 9, p. 2574, 2020.

[19] N. Yu, S. Zhao, X. Ma, Y. Wu, and R. Feng, "Effective Fingerprint Extraction and Positioning Method Based on Crowdsourcing," *Ieee Access*, vol. 7, pp. 162639-162651, 2019.

[20] N. Zhu, J. Marais, D. Bétaille, and M. Berbineau, "GNSS position integrity in urban environments: A review of literature," *Ieee T Intell Transp*, vol. 19, no. 9, pp. 2762-2778, 2018.

[21] K. Kotrotsios and T. Orphanoudakis, "Accurate Gridless Indoor Localization Based on Multiple Bluetooth Beacons and Machine Learning," 2021: IEEE, pp. 190-194

[22] P. Bahl and V. N. Padmanabhan, "RADAR: An in-building RF-based user location and tracking system," 2000, vol. 2: Ieee, pp. 775-784

[23] M. Youssef and A. Agrawala, "The Horus WLAN location determination system," presented at the Proceedings of the 3rd international conference on Mobile systems, applications, and services, Seattle, Washington, 2005. [Online].

[24] X. Guo, N. Ansari, L. Li, and H. Li, "Indoor Localization by Fusing a Group of Fingerprints Based on Random Forests," *IEEE Internet of Things Journal*, vol. 5, no. 6, pp. 4686-4698, 2018.

[25] W. Zhang, K. Liu, W. Zhang, Y. Zhang, and J. Gu, "Deep Neural Networks for wireless localization in indoor and outdoor environments," *Neurocomputing*, vol. 194, pp. 279-287, 2016/06/19/ 2016.

[26] Y. Li, Y. Zhuang, H. Lan, X. Niu, and N. El-Sheimy, "A Profile-Matching Method for Wireless Positioning," *Ieee Commun Lett*, vol. 20, no. 12, pp. 2514-2517, 2016.

[27] A. Brajdic and R. Harle, "Walk detection and step counting on unconstrained smartphones," 2013, pp. 225-234

[28] H. Weinberg, "Using the ADXL202 in pedometer and personal navigation applications," *Analog Devices AN-602 application note*, vol. 2, no. 2, pp. 1-6, 2002.

[29] W. Kang and Y. Han, "SmartPDR: Smartphone-Based Pedestrian Dead Reckoning for Indoor Localization," *Ieee Sens J*, vol. 15, no. 5, pp. 2906-2916, 2015.

[30] W. Shi, W. Ahmed, N. Li, W. Fan, H. Xiang, and M. Wang, "Semantic geometric modelling of unstructured indoor point cloud," *Isprs Int J Geo-Inf*, vol. 8, no. 1, p. 9, 2019.

[31] Z. Huang and J. Leng, *Analysis of Hu's moment invariants on image scaling and rotation*. 2010, pp. V7-476.

[32] S. Umeyama, "Least-squares estimation of transformation parameters between two point patterns," *IEEE Transactions on Pattern Analysis & Machine Intelligence*, vol. 13, no. 04, pp. 376-380, 1991.

[33] D. Munoz, F. Bouchereau, C. Vargas, and R. Enriquez, "CHAPTER 2 - Signal Parameter Estimation for the Localization Problem," in *Position Location Techniques and Applications*, D. Munoz, F. Bouchereau, C. Vargas, and R. Enriquez Eds. Oxford: Academic Press, 2009, pp. 23-65.

[34] S. J. Julier and J. K. Uhlmann, "Unscented filtering and nonlinear estimation," *P Ieee*, vol. 92, no. 3, pp. 401-422, 2004.

[35] X. M. Kang, B. Q. Huang, and G. D. Qi, "A Novel Walking Detection and Step Counting Algorithm Using Unconstrained Smartphones," (in English), *Sensors-Basel*, vol. 18, no. 1, Jan 2018.

[36] R. Chen, L. Pei, and Y. Chen, "A smart phone based PDR solution for indoor navigation," 2011, pp. 1404-1408

[37] A. Popleteev, "Indoor positioning and floor plan based ground truth: Can you really click where you are?," 2016,

Ahmed Mansour received his B.Sc. and M.Sc. degrees in civil engineering and Geomatics from Cairo University, Egypt, in 2013 and 2017, respectively. In 2017, he was awarded a Hong Kong Ph.D. Fellowship. His research interests include indoor positioning, multi-sensor fusion, crowdsourcing and cooperative positioning.

Junhua Ye received his Ph.D. degree in Geodesy and Surveying Engineering from Chang'an University in 2020 and currently works as a lecturer in the College of Environment and Resources at Zhejiang Agriculture and Forestry University. His research interests include multi-sensor fusion, agriculture, and forestry IoT.

Yaxin Li received his M.Sc. and Ph.D. degrees from the Department of Land Surveying and Geo-Informatics at the Hong Kong Polytechnic University, Hong Kong, in 2015 and 2020, respectively. He received his B.Sc. degree in Geomatics Engineering, School of Geodesy and Geomatics, Wuhan University, China, in 2013. His research interests include SLAM, indoor 3D modeling, semantic segmentation, and Auto BIM generation.

Huan Luo received her B.Sc. and M.Sc. degrees in Geomatics engineering from the Northeastern University, Shenyang, in 2013 and 2015, respectively. Since 2016, she has been a Ph.D. candidate in the department of Land Surveying and Geo-Informatics. Her research interests include GNSS navigation and multipath mitigation with low-cost devices.

Jingxian Wang received his B.Sc. and M.Sc. degrees from Nanjing University of Aeronautics and Astronautics, China, in 2015 and 2018, respectively. Currently, he is pursuing his Ph.D. in the Department of Land Surveying and Geo-Informatics, The Hong Kong Polytechnic University. His research interests include multi-information fusion and vehicle navigation.

Duojie Weng received his B.Sc. and M.Sc. degrees in electrical engineering from Hohai University, Nanjing, China, in 2007 and 2010, respectively, and the Ph.D. degree from the Hong Kong Polytechnic University in 2016. He is currently a post-doctoral researcher at the Hong Kong Polytechnic University. His research interests include GNSS integrity monitoring, kinematic GPS, and sensor integration.

Wu Chen is currently a professor and the head of the Department of Land Surveying and Geo-Informatics, The Hong Kong Polytechnic University. He has been actively working on GNSS-related research for more than 30 years. He has been working on many research projects funded by universities, governments, and industries. He has published over 300 technical papers in different journals and international conferences, submitted over 30 technical reports to various organizations, granted or filed more than ten patents. His main research interests include GNSS Applications on Transportation, Kinematic GPS, System Integration, GNSS Performance Evaluation, GPS Software Receiver, Regional GPS Network, Vehicle and Personal Navigation Systems, and Wireless Sensor Network.